Inorganic Chemistry

Article

pubs.acs.org/IC

Tuning the Rainbow: Systematic Modulation of Donor−Acceptor Systems through Donor Substituents and Solvent

Christopher B. Larsen,[†] Holly van der Salm,[†] Georgina E. Shillito, Nigel T. Lucas,* and Keith C. Gordon*

Department of Chemistry, University of Otago, P.O. Box 56, Dunedin, New Zealand

Supporting Information

ABSTRACT: A series of donor−acceptor compounds is reported in which the energy of the triarylamine donor is systematically tuned through para substitution with electron-donating methoxy and electron-withdrawing cyano groups. The acceptor units investigated are benzothiadiazole (btd), dipyridophenazine (dppz), and its $[ReCl(CO)_3(dppz)]$ complex. The effect of modulating donor energy on the electronic and photophysical properties is investigated using ^1H NMR spectroscopy, DFT calculations, electrochemistry, electronic absorption and emission spectroscopies, ground state and resonance Raman spectroscopy, and transient absorption spectroscopy. Qualitative correlations between the donor energy and the properties of interest are obtained using Hammett σ^+ constants. Methoxy and cyano groups are shown to destabilize and stabilize, respectively, the frontier molecular orbitals, with the HOMO affected more significantly than the LUMO, narrowing the HOMO−LUMO band gap as the substituent becomes more electron-donating—observable as a bathochromic shift in low-energy charge-transfer absorption bands. Charge-transfer emission bands are also dependent on the electron-donating/withdrawing nature of the substituent, and in combination with the highly solvatochromic nature of charge-transfer states, emission can be tuned to span the entire visible region.

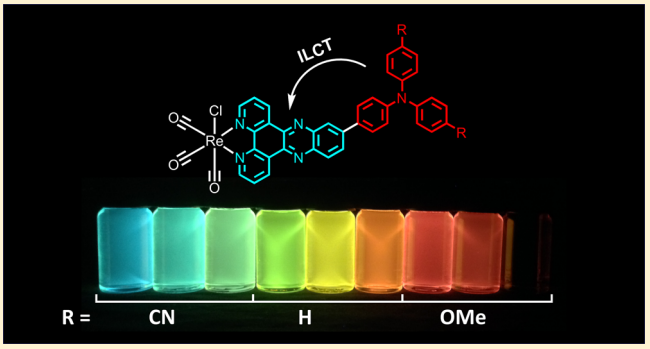

INTRODUCTION

Electron donor−acceptor (D−A) systems have been extensively investigated in recent years for their potential use in a wide range of molecular electronic,[1,2] photovoltaic,[3−5] and biological imaging applications.[6] Their utility in such systems is a function of their frontier molecular orbitals, where occupied orbitals are localized on the donor unit and unoccupied orbitals on the acceptor unit.[7−9] Upon photoexcitation with ultraviolet, visible, or near-infrared irradiation, an electron is donated from the donor to the acceptor in a charge-transfer (CT) process.

Due to the localized nature of the donor and acceptor orbitals, the energy of a CT electronic transition depends on the energy levels of each component and can be tuned through alteration of either one or both of these components. Tuning the energy of the CT transition has often involved substitution of[10,11] or replacing[12−15] the acceptor unit. In order to allow experimental results to guide the rational design of future materials with predictable properties, studies must be systematic. Examples of energetics tuning are the modification of benzo[*c*][1,2,5]thiadiazole to give periodic analogues—replacing S with Se results in a smaller electrochemical band gap and, consequently, a bathochromic shift of both absorption and emission CT bands[16,17] and tuning of the acceptor energy through extension of conjugation.[18]

In addition to replacing the donor unit,[19] a number of studies use π-conjugated bridges to tune the donor energy.[20,21] However, the use of peripheral substituents to systematically tune donor energies, analogous to studies on modulating acceptor energies,[10,11] is underrepresented in the literature.

Re(I), Cu(I), and Ru(II) dipyridophenazine (dppz) complexes appended with sulfur-based donors have also exhibited interesting electronic properties with respect to donor energy. $[ReCl(CO)_3(dppz)]$ and $[Cu(bpy(Mes)_2)(dppz)]^+$ complexes appended with weak thioether or trithiocarbonate donors exhibit dual intraligand/metal-to-ligand (IL/MLCT) transitions,[22,23] while $[Ru(bpy)_2(dppz)]^{2+}$ complexes appended with strong tetrathiafulvalene donors exhibit independent ILCT and MLCT transitions of significantly different energy.[24] Systematic modulation of donor energy may shed light on such phenomena.

The energy of MLCT and π,π^* transitions has been successfully tuned in a predictable manner using substitution effects.[25−31] These studies have utilized Hammett constants (σ) for substituted benzene derivatives, typically used to estimate the chemical reactivity of a site, to model the electronic influence of the substituent. These constants are not universally applicable; there are specific constants for meta- vs para-substituted systems (σ_m and σ_p, respectively) as well as for reactions in which the substituent is in resonance with the site

Received: April 29, 2016

DOI: 10.1021/acs.inorgchem.6b01039
Inorg. Chem. XXXX, XXX, XXX−XXX

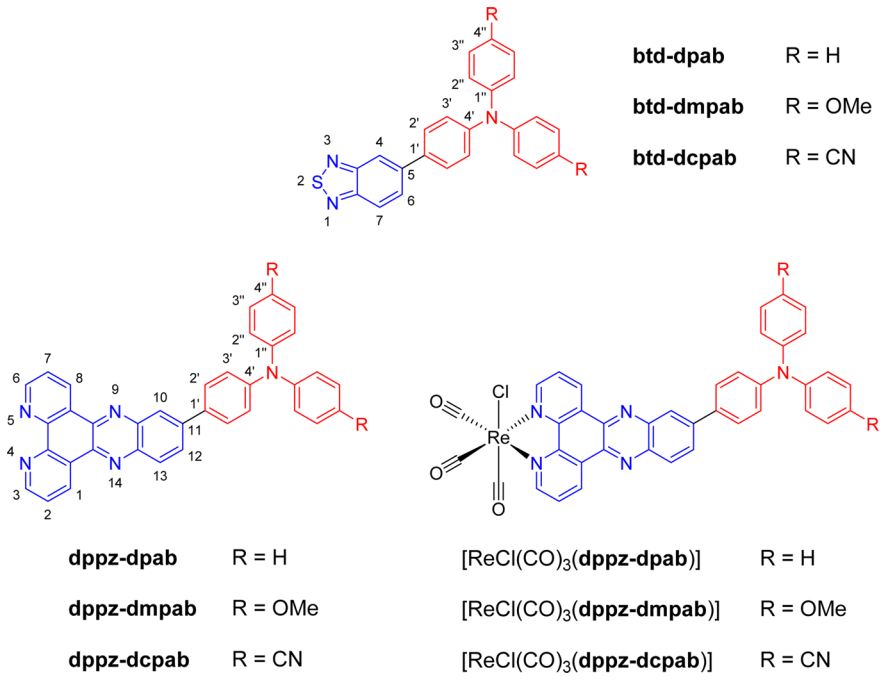

Figure 1. Compounds investigated in this study and naming convention used. Donor is depicted in red and acceptor in blue. Reactions described as overnight typically had a duration of 15 h.

of reaction (σ^- for when the reaction site becomes electron rich and σ^+ for when the reaction site becomes electron deficient).[32] With respect to D−A systems, σ^- is appropriate for describing substitution effects on the acceptor (which receives an electron upon photoexcitation) and σ^+ for the donor (which loses an electron upon photoexcitation).

In this study, the triarylamine (TAA) donor is substituted at the para positions with electron-withdrawing cyano (R = CN, dcpab, $\sigma^+ = 0.659$) and electron-donating methoxy groups (R = OMe, dmpab, $\sigma^+ = -0.778$) and compared to the unsubstituted TAA donor (R = H, dpab, $\sigma^+ = 0.000$). Three acceptors previously investigated are utilized in this study: benzothiadiazole (btd),[1] the dipyridophenazine (dppz) ligand,[9] and its [ReCl(CO)$_3$(dppz)] complex (Figure 1).[33] The [ReCl(CO)$_3$(dppz)] complex is of particular interest, as the presence of the metal potentially allows competitive CT processes with either the TAA donor or metal-donating electron density to the dppz ligand, ILCT and MLCT, respectively.[9,22,33−35] MLCT transitions can be identified through the enhancement of carbonyl stretching modes in resonance Raman spectra.[9,22,33,34,36,37] Electronic and photophysical properties are qualitatively correlated to the σ^+ Hammett constant and characterized using ^{1}H NMR spectroscopy, DFT calculations, electrochemistry, electronic absorption and emission spectroscopies, ground state and resonance Raman spectroscopy, and transient absorption spectroscopy.

RESULTS AND DISCUSSION

Synthesis and Crystallography. Synthetic routes toward the target compounds are outlined in Scheme 1. btd-dmpab was obtained in three steps from 5-bromobenzo[*c*][1,2,5]-thiadiazole (btd-Br) using Suzuki−Miyaura coupling with 4-trimethylsilylphenylboronic acid to afford a trimethylsilylphenyl-substituted btd; the trimethylsilyl groups acts as a masked halide and is converted to an iodo group in good yield through iododesilylation with ICl. The resulting iodo group is then reacted in a Buchwald−Hartwig coupling with di(4-methoxyphenyl)amine to afford btd-dmpab in good yield.

The synthesis of btd-dcpab could not be realized in a manner analogous to btd-dmpab, due to btd-dcpab and di(4-cyanophenyl)amine being chromatographically inseparable. However, it was identified that a key step in the preparation of di(4-cyanophenyl)amine from diphenylamine was selective iodination at the 4-positions. As the btd ring is electron poor, it was believed that iodination of btd-dpab, obtained in one high-yielding step from btd-Br, would occur selectively at the 4 positions of the TAA donor. This was proved correct, selectively affording the desired product in excellent yield. Rosenmund−von Braun cyanation affords btd-dcpab in good yield.

btd-dpab and btd-dmpab were converted into dppz-dpab and dppz-dmpab, respectively, using $LiAlH_4$ reduction and sulfur extrusion, followed by Schiff-base condensation with 1,10-phenanthroline-5,6-dione. Cyano groups are sensitive to $LiAlH_4$ reduction; $CoCl_2$-catalyzed $NaBH_4$ reduction, followed by Schiff-base condensation successfully affords dppz-dcpab in 41% yield. Re(I) complexation was achieved in good to excellent yields using standard methods.

An X-ray crystal structure was obtained using a crystal obtained from slow evaporation of a $CHCl_3$ solution of dppz-dmpab (Figure 2). dppz-dmpab crystallized in the *P*-1 space group, cocrystallizing with one molecule of $CHCl_3$ per molecule of dppz-dmpab. The dppz skeleton is essentially planar, with a maximum deviation from planarity at C18 of 0.14 Å, as is the donor amine, with N5 lying 0.09 Å above a plane defined by the ipso carbons (C22, C25, and C31). As with previous reports of dppz ligands,[9,34] the cocrystallized $CHCl_3$ hydrogen bonds with the phenanthroline-type nitrogens in a bifurcated manner (2.29 Å to N1 and N2). The crystal structure and DFT-optimized structure agree well, with an average difference in bond length of 0.006 Å. The donor unit is predicted to be rotated 31.4° from the dppz and is

DOI: 10.1021/acs.inorgchem.6b01039
Inorg. Chem. XXXX, XXX, XXX−XXX

Scheme 1. Synthesis of Target Compounds[a]

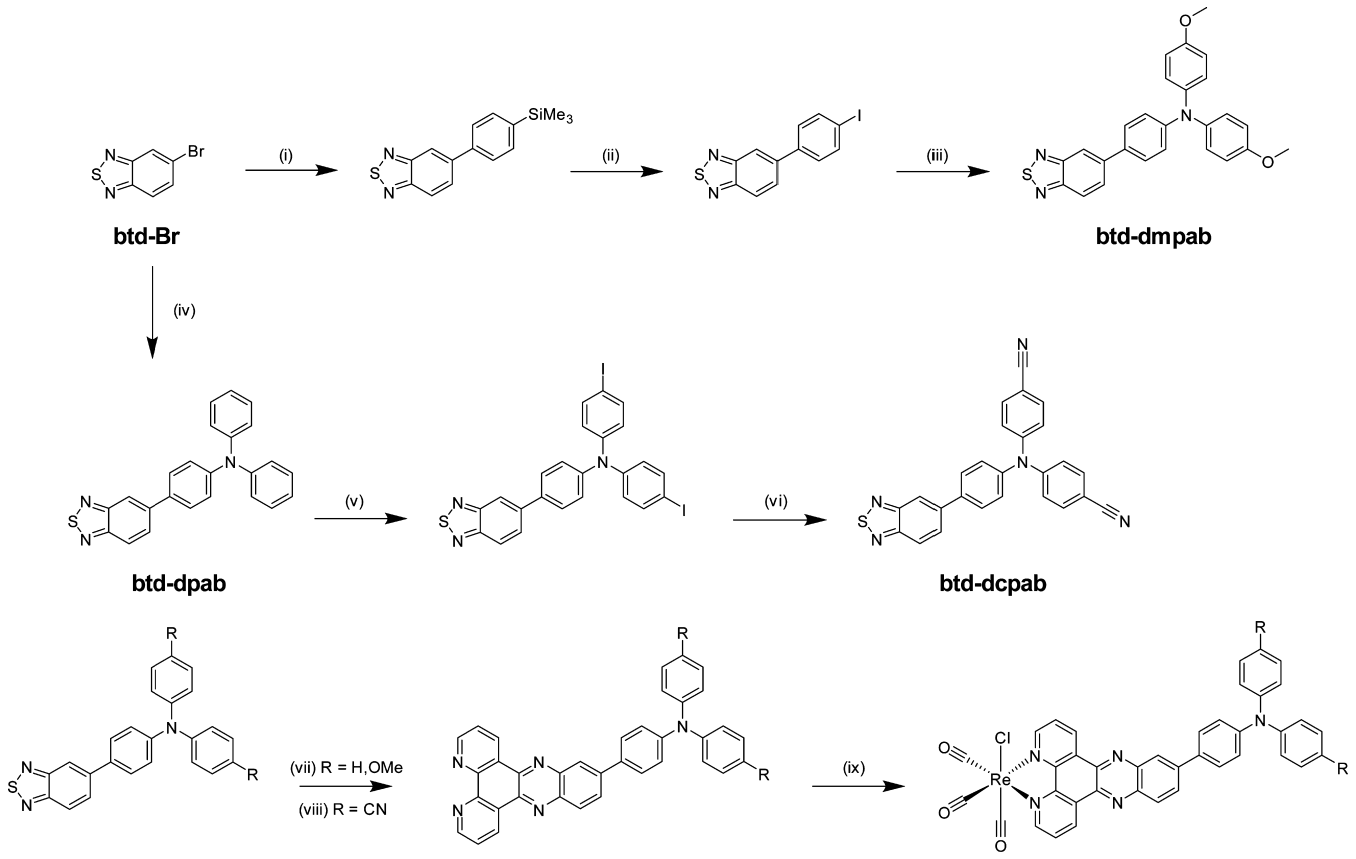

[a](i) 4-Trimethylsilylphenylboronic acid, K_2CO_3, $PdCl_2$(dppf), toluene, water, EtOH, reflux, 15 h, 87%; (ii) ICl, CH_2Cl_2, −78 °C, 2 h, 89%; (iii) di(4-methoxyphenyl)amine, ^tBuOK, $[^tBu_3PH]BF_4$, $Pd_2(dba)_3$, toluene, reflux, 15 h, 61%; (iv) 4-diphenylaminophenylboronic acid, K_2CO_3, $PdCl_2$(dppf), toluene, water, EtOH, reflux, 15 h, 94%; (v) KI, KIO_3, AcOH, water, 80 °C, 14 h, 93%; (vi) CuCN, DMF, reflux, 15 h, 84%; (vii) (a) $LiAlH_4$, THF, rt, 15 h; (b) 1,10-phenanthroline-5,6-dione, EtOH, reflux, 15 h, 39% (R = H), 32% (R = OMe); (viii) (a) $NaBH_4$, $CoCl_2$, EtOH, reflux, 15 h; (b) 1,10-phenanthroline-5,6-dione, EtOH, reflux, 15 h, 41%; (ix) $[ReCl(CO)_5]$, EtOH, reflux, 15 h, 91% (R = H), 78% (R = OMe), 45% (R = CN).

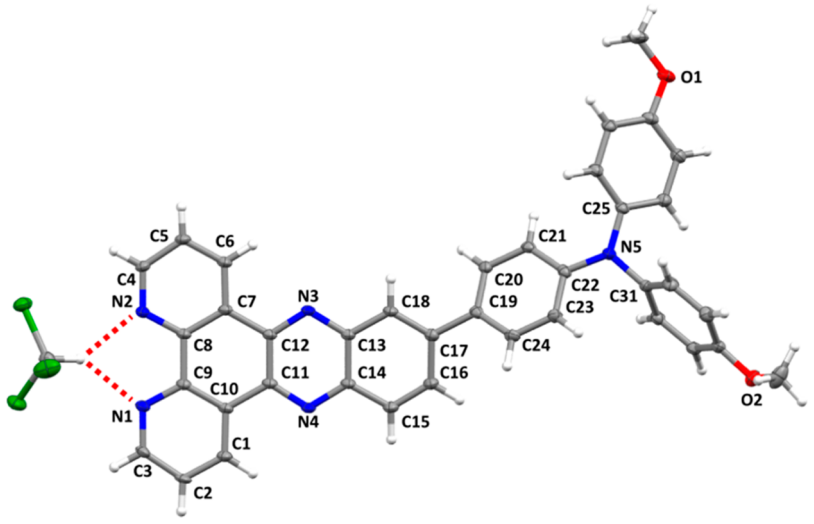

Figure 2. X-ray crystal structure of dppz-dmpab. Ellipsoids are shown at 50% probability level.

experimentally observed as 32.3°. One terminal donor phenylene shows good agreement between calculated and experimental torsion angles (70.9° versus 71.9°, respectively). The other terminal donor phenylene is predicted to be rotated further out of plane than is observed experimentally (62.8° versus 48.7°, respectively), likely due to solid state packing interactions not modeled in the DFT-optimized structure. An X-ray crystal structure of the trimethylsilylphenyl-substituted btd intermediate was obtained from ethanol recrystallization

DOI: 10.1021/acs.inorgchem.6b01039
Inorg. Chem. XXXX, XXX, XXX−XXX

and crystallized in the *P*-1 space group (see Supporting Information).

^{1}H NMR Spectroscopy. In the ^{1}H NMR spectra, the chemical shift (δ) of protons in resonance with the substituent show significant shifts and may be related to the Hammett constant,[38,39] while protons not in resonance do not shift significantly (Figure 3). Electron-donating substituents increase

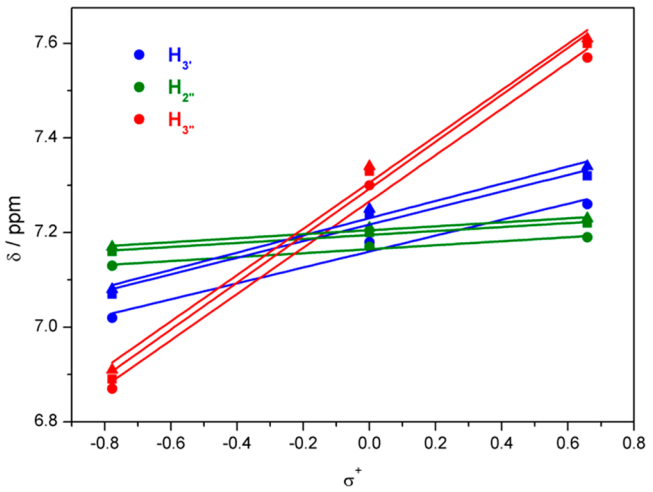

Figure 3. Correlation between ^{1}H NMR chemical shifts (500 MHz, $CDCl_3$) of donor group protons: btd (●), dppz (■), and [$ReCl(CO)_3$(dppz)] (▲).

the electron density at positions in resonance with the substitution, effectively shielding those protons and imbuing an upfield shift. Conversely, electron-withdrawing substituents decrease electron density at those positions, deshielding those protons and eliciting a downfield shift. Thus, the overall effect on resonant protons is a downfield shift with increasing σ^+.

For the donor group protons, $H_{3''}$ (numbering scheme depicted in Figure 1) shows the greatest effect, while $H_{3'}$ (with a longer resonance pathway) shows a weaker effect, and $H_{2''}$ (not in resonance) shows almost no effect. $H_{2'}$ is not in resonance with the substituent and is also affected by through-space interaction with acceptor protons and therefore shows no trend. Importantly, these trends are consistent across the range of acceptors, indicating that only the substituent influence on the donor energy is being probed.

Interestingly, acceptor group protons also exhibit some sensitivity to the substituent (Tables S1 and S2), with the protons positioned ortho to the imine nitrogens (H_4 and H_7 for the btd systems, H_{10} and H_{13} for the dppz ligands and complexes) shifting at the same magnitude, implying that donor substitution also affects acceptor energy to a certain extent. The proton position ortho to the donor but not to an imine nitrogen (H_6 for btd systems, H_{12} for dppz ligands and complexes) shows no sensitivity to substituent, however. For the dppz ligands and complexes, phen-type protons also show slight shifts with substituent.

FT-Raman Spectroscopy. Experimental FT Raman and calculated Raman spectra for dppz ligands and their respective Re(I) complexes are presented in Figure S1; an example is presented in Figure 4. Spectra could not be obtained for btd compounds due to intense emission from these samples. Calculated spectra are scaled in order to minimize the mean absolute deviation (MAD) in frequency to the experimental spectra. MAD values can be used to validate DFT calculations;

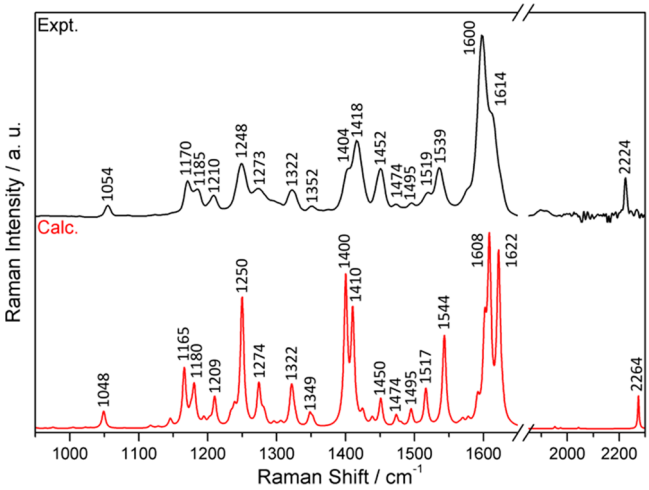

Figure 4. FT-Raman spectra (solid sample, λ_{ex} = 1064 nm, black) and DFT-calculated spectra (in vacuo B3LYP, red) of [$ReCl(CO)_3$(dppz-dcpab)].

values of ≤10 cm^{-1} are considered a good fit.[9,22,33,34,36,40−43] MAD values for the dppz ligands and complexes range from 4 to 7 cm^{-1} (Table S3).

Some strong similarities can be observed between all spectra: all of the ligands show a strong band around 1410 cm^{-1} typical of dppz, which is a vibrational mode of the phenazine (phz) part of the molecule, and also show the strongest modes around 1600 cm^{-1} which are associated with the TAA;[9] these modes are also consistently calculated. The 1410 cm^{-1} phenazine mode does not shift between the ligands, in either experimental or calculated spectra, which is unsurprising due to the distance between the phz part of the molecule and the substitution. However, there are small shifts observed in the TAA-based modes, although in both experimental and calculated spectra the addition of either OMe or CN groups shifts the bands to ∼6 cm^{-1} higher in frequency. This appears to be a mass effect as simulating a heavy mass (via a H atom with mass 12) gives a predicted upshifted wavenumber also. A similar effect is observed for the Re(I) complexes, with little shift in the phz mode between compounds, and a shift to higher frequency of ∼6 cm^{-1} for the TAA-based modes around 1600 cm^{-1}. Modes around 1520 cm^{-1} also exhibit a relative increase in intensity for complexes but only minimal shifting in frequency for experimental spectra; this mode is predominantly associated with the phenylene linker.

Electrochemistry. Cyclic voltammetry data may be used to estimate the energies of frontier molecular orbitals (FMOs) using the method of Li et al.[44] Electrochemical data and estimated FMO energies are presented in Table S6. DFT calculations (B3LYP, in vacuo) predict the HOMO to be localized on the TAA donor and the LUMO on the acceptor for all investigated compounds (Tables S7−S9). The electrochemical band gap ($E_{LUMO-HOMO}$) widens with increasing σ^+ for each acceptor system, with the different acceptors offsetting this trend (Figure S2). This is consistent with the substituent significantly modulating donor energy and having a smaller effect on acceptor energy, as implied by ^{1}H NMR spectroscopy. DFT calculations accurately predict these two trends (Figure 5), giving confidence in DFT-based assignments. It is interesting to note that although the HOMO−1 for the dppz complexes is predicted to be metal based, the energy of this orbital is predicted to show a slight dependence on substituent.

DOI: 10.1021/acs.inorgchem.6b01039
Inorg. Chem. XXXX, XXX, XXX−XXX

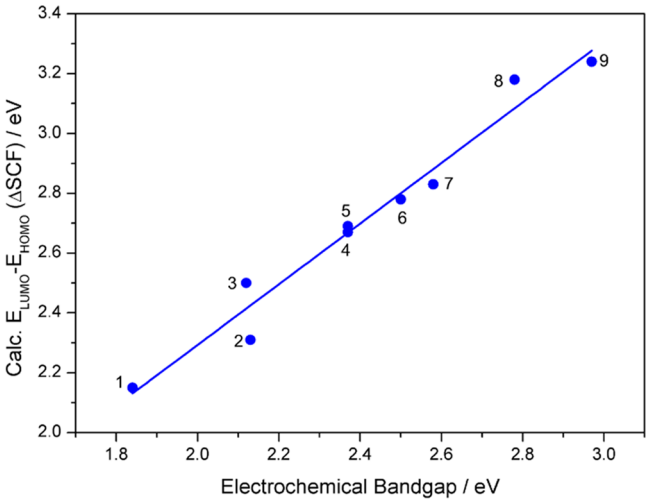

Figure 5. Relationship between electrochemical band gap (recorded in CH_2Cl_2) and DFT-predicted HOMO−LUMO band gap (CH_2Cl_2 solvent field). Points correspond to (1) [ReCl(CO)$_3$(dppz-dmpab)], (2) [ReCl(CO)$_3$(dppz-dpab)], (3) dppz-dmpab, (4) btd-dmpab, (5) dppz-dpab, (6) [ReCl(CO)$_3$(dppz-dcpab)], (7) btd-dpab, (8) dppz-dcpab, (9) btd-dcpab. Tabulated data are in Supporting Information Tables S6 and S10.

Electronic Absorption Spectroscopy. Electronic absorption spectra are presented in Figure 6. For all acceptor systems, the lowest energy absorption band (previously assigned as ILCT in nature)[9] hypsochromically shifts with increasing σ^+. For the btd compounds, this shift results in a lack of a clear low-energy band for btd-dcpab. In addition to the electronic influence of the substituent on the donor unit altering the energy of absorption, the nature of the acceptor is also significant, with btd compounds absorbing at higher energy relative to dppz, while Re(I) complexation of dppz ligands further lowers the energy of absorption. Higher energy absorption bands do not show the same dependence on σ^+ and are assigned as acceptor-localized π,π^* bands. btd-dcpab exhibits another low-energy band (~350 nm) not present in the other btd compounds; this band occurs at the same energy and therefore is convoluted with the dppz-localized π,π^* bands in the dppz ligands and complexes. The lack of variation in the energy of this band across the investigated acceptors implies that this band is a TAA-localized π,π^* or a TAA → CN CT transition as recently reported by Easwaramoorthi et al.[45]

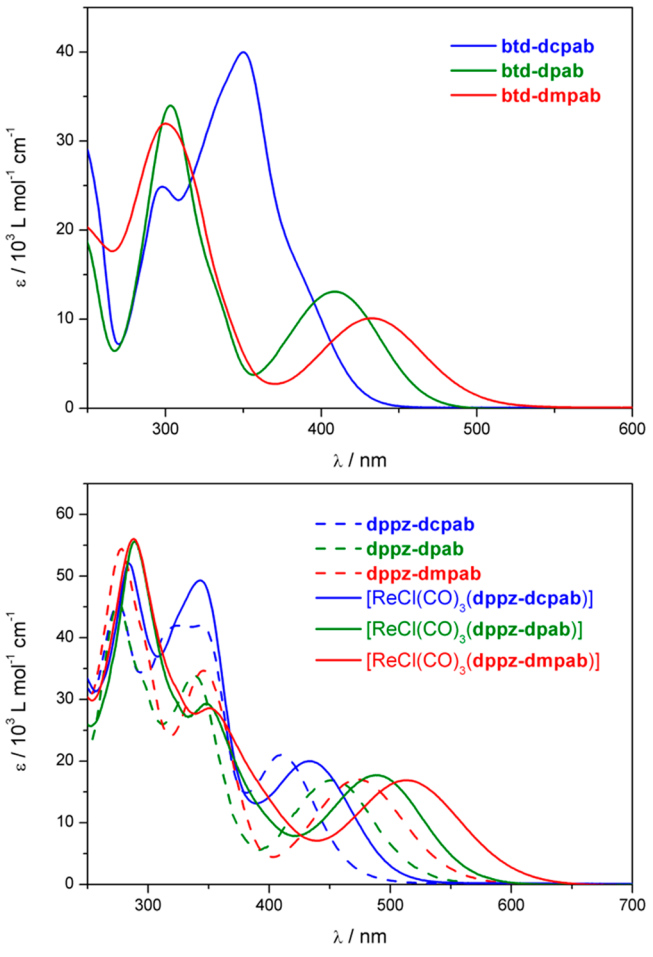

Figure 6. Electronic absorption spectra, recorded in CH_2Cl_2.

A plot of the energy of absorption (E_{abs}) against the electrochemically estimated HOMO−LUMO band gap (excluding btd-dcpab for which E_{abs} could not be defined) shows a linear correlation (Figure 7). This is consistent with a HOMO → LUMO transition, as predicted by TD-DFT calculations (vide infra), and shows that the electronic influence of the substituent affects both E_{abs} and the electrochemical band gap by altering the donor energy but not changing the nature of the transition. This finding is closely analogous to early work on tuning the energy of MLCT transitions in Re(I) and Ru(II) polypyridyl complexes, in which the optical band gap was related to changes in the reduction potential of the complex upon substitution of the polypyridyl ligand.[46,47]

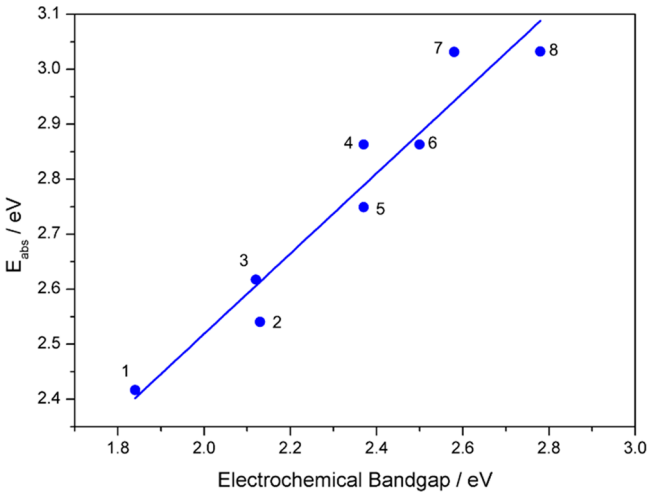

Figure 7. Correlation between the experimental E_{abs} of the ILCT absorption band and the electrochemical band gap, both recorded in CH_2Cl_2. Points correspond to (1) [ReCl(CO)$_3$(dppz-dmpab)], (2) [ReCl(CO)$_3$(dppz-dpab)], (3) dppz-dmpab, (4) btd-dmpab, (5) dppz-dpab, (6) [ReCl(CO)$_3$(dppz-dcpab)], (7) btd-dpab, (8) dppz-dcpab. Tabulated data are in Supporting Information Tables S6 and S11.

Both B3LYP and CAM-B3LYP TD-DFT calculations successfully reproduce the experimental trends of bathochromically shifting absorption for the lowest energy absorption band as the substituent becomes more electron donating and that for a given substituent absorption also bathochromically shifts as the acceptor is changed from dppz to [ReCl(CO)$_3$(dppz)]

DOI: 10.1021/acs.inorgchem.6b01039
Inorg. Chem. XXXX, XXX, XXX−XXX

(Figure 8). B3LYP and CAM-B3LYP calculations predict HOMO → LUMO transitions (Figure 9) for the lowest energy

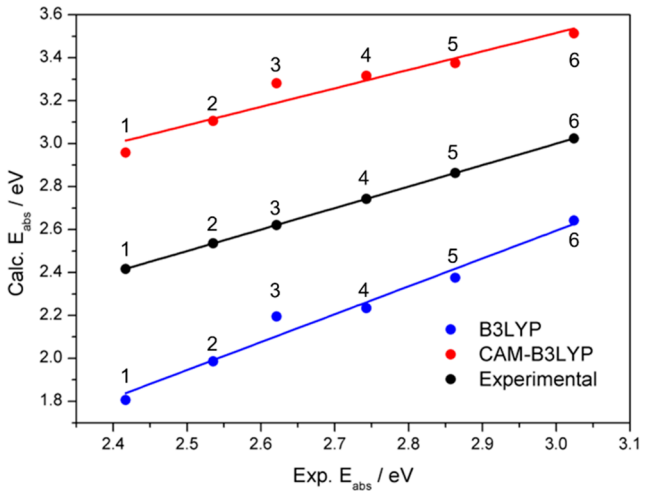

Figure 8. Correlation between predicted (TD-DFT, CH_2Cl_2) and experimental E_{abs} (recorded in CH_2Cl_2) for the ILCT absorption band. Slopes are all the same within experimental error (1.0 ± 0.2). Points correspond to (1) [ReCl(CO)$_3$(dppz-dmpab)], (2) [ReCl(CO)$_3$(dppz-dpab)], (3) dppz-dmpab, (4) dppz-dpab, (5) [ReCl(CO)$_3$(dppz-dcpab)], (6) dppz-dcpab. Tabulated data are in Supporting Information Tables S11 and S12.

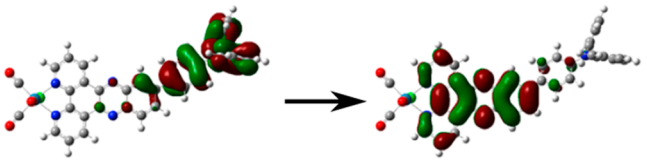

Figure 9. HOMO → LUMO transition for [ReCl(CO)$_3$(dppz-dpab)] predicted by CAM-B3LYP TD-DFT calculations (with CH_2Cl_2 solvent field).

absorption band (Tables S11 and S12). The Mulliken charge density change modeled using CAM-B3LYP shows negligible contribution from the metal to the lowest energy charge transfer transition, with little change observed between the complexes, supporting assignment of an ILCT transition (Table S12).

Resonance Raman Spectroscopy. Resonance Raman spectroscopy, in which the laser excitation wavelength is coincident with an electronic transition and vibrational modes enhanced are associated with the active chromophore,[48] can be used to qualitatively assign the nature of transitions by the nature of bands enhanced. This may be used as an experimental validation of TD-DFT calculations. Resonance Raman spectra of the three dppz complexes are presented in Figure 10. We previously characterized the behavior of [ReCl(CO)$_3$(dppz-dpab)] as ILCT in nature and by virtue of only subtle spectral changes across excitation wavelengths concluded that the ILCT transition was dominant across all excitation wavelengths.[9] The spectra of [ReCl(CO)$_3$(dppz-dmpab)] show some similar enhancement patterns to [ReCl(CO)$_3$(dppz-dpab)], but for [ReCl(CO)$_3$(dppz-dcpab)] there are spectral differences, and these become more obvious as the excitation wavelength is changed. The key enhancements for [ReCl(CO)$_3$(dppz-dcpab)] at wavelengths coinciding with the lowest energy absorption band are observed at 1600 and 1539 cm^{-1}, which are assigned as TAA and dppz based modes, respectively. This is consistent with an ILCT transition from the TAA-localized HOMO to a dppz-based LUMO. This assignment is also supported by TD-DFT calculations. The 1539 cm^{-1} vibration is largely associated with the phz component of the dppz ligand; however, the addition of the TAA substituent to dppz perturbs the individual phen and phz molecular orbitals; hence, other dppz-based modes at 1248, 1322, 1352, 1418, 1452, and 1578 cm^{-1} are also enhanced in the transition.

As the excitation wavelength shortens and starts to coincide with the higher energy absorption band, these dppz-localized vibrations become further enhanced, as does a TAA mode at 1614 cm^{-1}, which is consistent with both dppz-localized and TAA-localized π,π^* transitions. With 351 nm excitation, two additional modes are further enhanced at 1170 and 2224 cm^{-1}, assigned as TAA and CN vibrations, respectively, indicative of a TAA-localized π,π^* or TAA → CN transition as recently reported by Easwaramoorthi et al.[45] This is supported by TD-DFT calculations which predict a significant contribution to the transition from the HOMO to the LUMO+3, with the LUMO +3 localized on the terminal phenylene rings and cyano substituents of the donor.

For [ReCl(CO)$_3$(dppz-dmpab)], similar enhancements to [ReCl(CO)$_3$(dppz-dcpab)] are observed at wavelengths coinciding with the lowest energy absorption band. Key enhancements at 1535 and 1165 cm^{-1} are associated with predominantly phz-localized LUMO and TAA-localized HOMO vibrations, respectively, and are therefore consistent with a HOMO → LUMO transition. Analogous to [ReCl(CO)$_3$(dppz-dcpab)], dppz-localized modes at 1245, 1322, 1349, 1405, 1450, and 1577 cm^{-1} are also enhanced. At 406 and 413 nm, very small enhancement of carbonyl modes at 2026 cm^{-1} is observed (also observed for [ReCl(CO)$_3$(dppz-dpab)] at 2027 cm^{-1}), consistent with marginal contribution from an MLCT transition. Interestingly, this is not observed for [ReCl(CO)$_3$(dppz-dcpab)]. Mulliken analysis of CAM-B3LYP calculations shows a contribution from the metal to the lowest energy transition of 6%, 0%, and 4% for [ReCl(CO)$_3$(dppz-dcpab)], [ReCl(CO)$_3$(dppz-dpab)], and [ReCl(CO)$_3$(dppz-dmpab)], respectively.

The similarity between the resonance Raman spectra of the complexes at excitation wavelengths coinciding with the lowest energy absorption band implies that while the substituent tunes the energy of the transition it has no effect on the electronic nature of the transition.

Emission Spectroscopy. All compounds exhibit highly solvatochromic emission that is insensitive to the presence of $^3O_2$, consistent with ^{1}ILCT emissive states,[9] even for the complexes, which often exhibit triplet-state emission due to efficient intersystem crossing facilitated by the metal.[34] As with the CT absorption bands, λ_{em} shows a strong dependence on the substituent, and in combination with the strong solvatochromism of each compound, emission can be tuned to span the entire visible region (Figure 11). It is clear that in many cases there is more than one emissive state and that these can show switching as illustrated in Figure S3. For the data shown, the second emissive state can be seen in plot 9 of Figure 11. A plot of E_{em} for the CT emission bands against the electrochemical band gap is linear (Figure 12), indicating that emission is occurring from the absorbing state and λ_{em} can therefore be rationally tuned using Hammett constants.

DOI: 10.1021/acs.inorgchem.6b01039
Inorg. Chem. XXXX, XXX, XXX−XXX

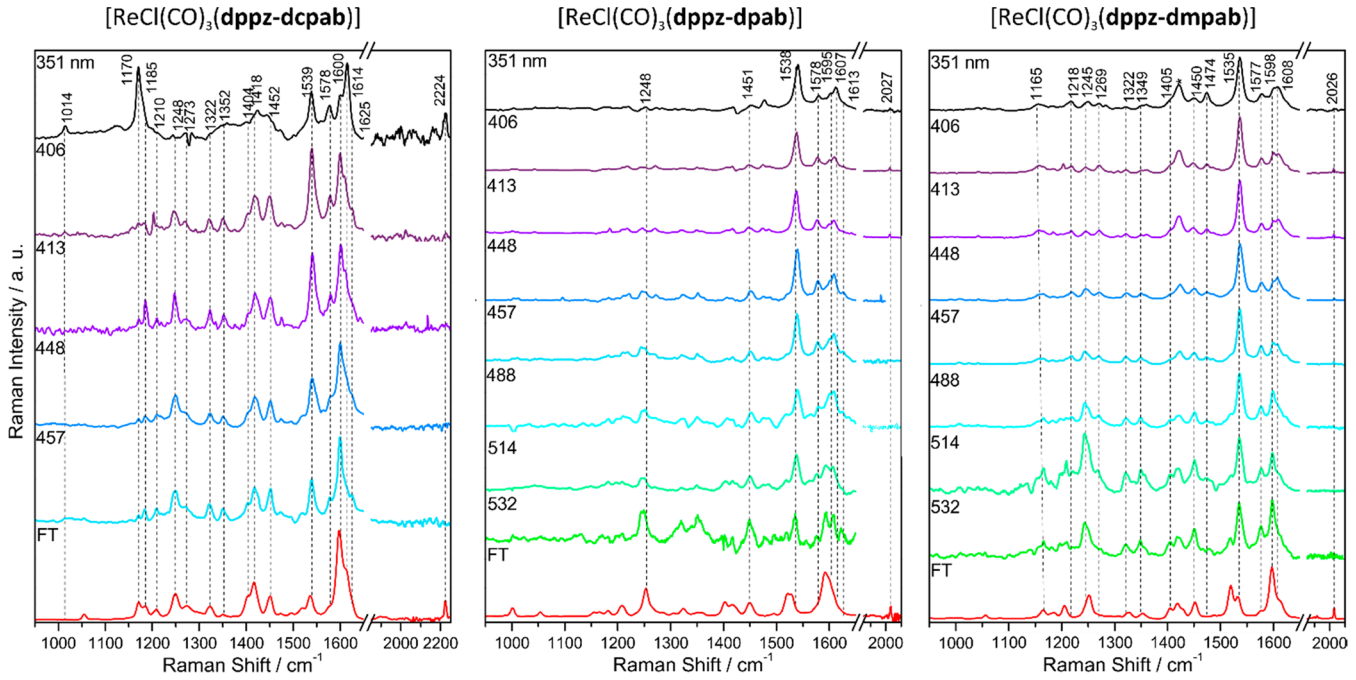

Figure 10. Resonance Raman spectra of dppz complexes, recorded in CH_2Cl_2 (1 mM) at a range of excitation wavelengths, and FT-Raman spectra (solid state, 1064 nm excitation).

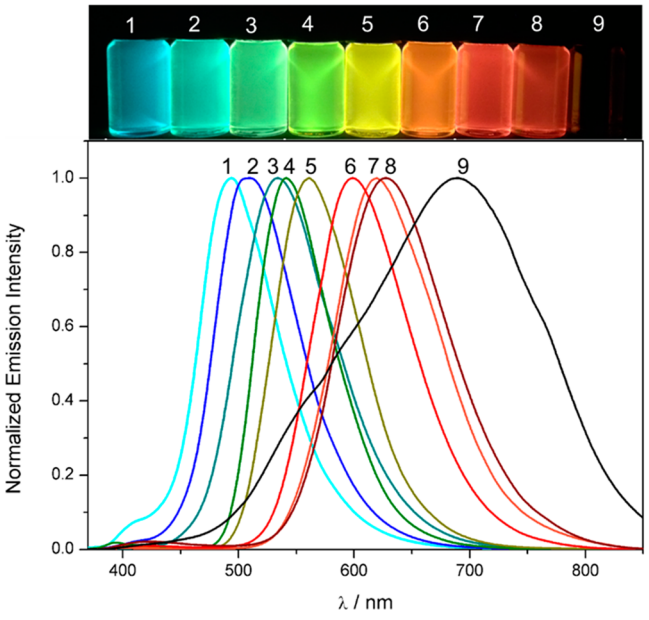

Figure 11. Emission of dppz-dcpab in toluene (1), 1,4-dioxane (2), and $CHCl_3$ (3), dppz-dpab in toluene (4), 1,4-dioxane (5), and $CHCl_3$ (7), and dppz-dmpab in toluene (6), 1,4-dioxane (8), and $CHCl_3$ (9).

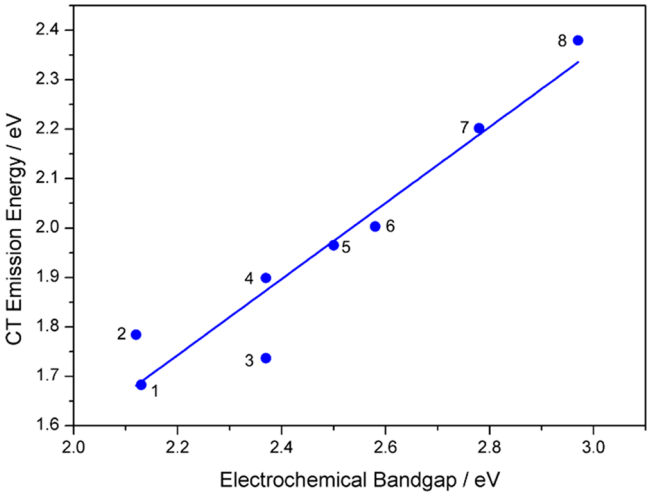

Figure 12. Relationship between electrochemical band gap and energy of emission for CT bands recorded in CH_2Cl_2. Points correspond to (1) [ReCl(CO)$_3$(dppz-dpab)], (2) dppz-dmpab, (3) btd-dmpab, (4) dppz-dpab, (5) [ReCl(CO)$_3$(dppz-dcpab)], (6) btd-dpab, (7) dppz-dcpab, (8) btd-dcpab.

TD-DFT was used to calculate the emission energies of the dppz ligands, presented in Table S13. The excited state structures were optimized in different solvents using the integral equation formalism (IEF) version of the polarizable continuum model (PCM) with both B3LYP and CAM-B3LYP functionals using the 6-31G(d) basis set. The default linear response (LR) solvent parameter was employed due to its computational efficiency and that a precise, quantitative analysis of the emission energies of the compounds was not required for this investigation. However, in recent years there has been significant development of more sophisticated computational methods by which solvent−solute polarization is more accurately modeled.[49−53] For instance, the state-specific (SS) formalism can be applied to the PCM model, in which the solvent electrostatically responds to electron density of the excited state, whereas with LR only the response of the solvent with respect to the ground state electron density is considered. The SS approach therefore provides a more reliable representation of the polarization of the solvent in response to formation of the excited state.[50,51,54,55]

A number of studies have compared LR and SS approaches for calculating vertical excitation and emission energies of different compounds in solution.[50,51,54,56] Improta et al. compared the emission energies of coumarin derivatives in

DOI: 10.1021/acs.inorgchem.6b01039
Inorg. Chem. XXXX, XXX, XXX−XXX

ethanol calculated with PCM/TD-DFT using SS and LR models.[50] The study showed that the SS model gave predicted values very close to the experimentally observed emission energies; however, it also showed that the LR method was able to provide qualitative estimates. Guido et al. compared the TD-DFT-calculated absorption and emission spectra of Nile Red using a range of functionals and polarization schemes.[57] They showed that due to error cancellation, accurate results were obtained if LR was used with B3LYP and also when SS was used with CAM-B3LYP. This is feasibly what is observed in this case, as the emission energies predicted using B3LYP are a closer match to the experimental data than those predicted using CAM-B3LYP (Table S13).

A series of donor−acceptor dyes, also containing TAA donor substituents, was studied by Bernini et al.[58] The emission energies were calculated using TD-DFT in conjunction with wide variety of functionals, basis sets, and polarization schemes. When range-separated hybrid functionals are used with LR, the mean absolute error between the calculated and the experimental emission energies is approximately 0.2 eV and reduced to 0.15 eV when the SS approach is utilized. These studies highlight the importance of the selection of functional, basis set, and polarization scheme in regard to the type of transition that is occurring if precise, quantitative analysis is desired.

For the purpose of our investigation the LR method was satisfactory as the calculations successfully reproduce the trend of increasing λ_{em} as the TAA substituent becomes more electron donating and support assignment of an ILCT emissive state. This trend is observed in both solvents modeled. In general, the λ_{em} values modeled in chloroform were predicted at longer wavelengths than those in toluene, as seen experimentally. A reasonable correlation with experimental data was observed from results obtained using B3LYP. Although the trend in λ_{em} was correctly modeled using CAM-B3LYP, the predicted values were significantly offset.

Transient Absorption Spectroscopy. Transient absorption (TA) spectroscopy provides the absorption spectrum of the longer-lived (ns) excited states, and the excited state lifetimes can also be determined by measuring the decay of the signal. Emission lifetimes are too short to be measured on the available instrumentation, indicating that two different states are being probed: the ^{1}ILCT for the emission and a ^{3}ILCT dark state for the transient absorption as previously seen for [ReCl(CO)$_3$(dppz-dpab)].[9]

The lifetimes of the three dppz complexes appear to be the same within experimental error (Table 1). Consequently, the differences in the electronic nature of the substituents on the TAA donor are not enough to perturb the decay of the excited state.

In addition, the transient absorption spectra are all very similar (Figure 13) with bleaching of the ground state at ∼360 and 450−500 nm and positive absorption of the excited state at ∼420 nm and at wavelengths longer than 500 nm. This indicates that the long-lived dark state in these compounds is likely to be similar in nature for all three, and the presence of the broad absorption band at low energy is consistent with an oxidized TAA unit,[9,59,60] consistent with this being a ^{3}ILCT state. In addition, the reported spectra for phen$^{\bullet-}$ show absorption features in this region.[61]

Table 1. Dark State Lifetimes

compound	τ (μs)
[ReCl(CO)$_3$(dppz-dcpab)]	3.0 ± 0.8
[ReCl(CO)$_3$(dppz-dpab)]	3.8 ± 0.4
[ReCl(CO)$_3$(dppz-dmpab)]	3.6 ± 0.1

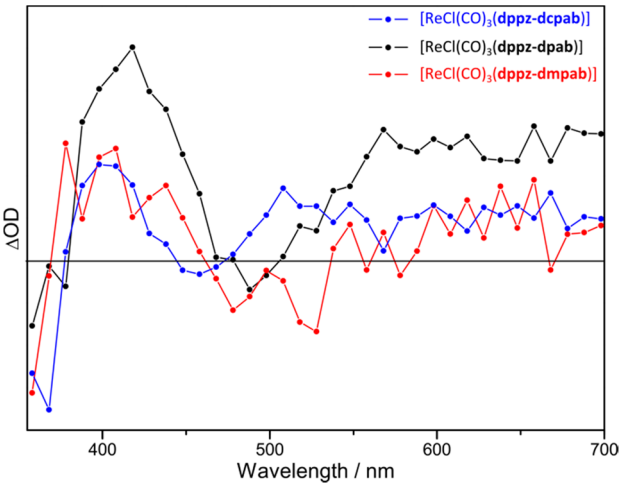

Figure 13. Transient absorption spectra of dppz complexes in CH_2Cl_2, recorded 200 ns after 355 nm excitation.

CONCLUSIONS

In order to systematically probe the effect of donor energy on the D−A behavior, compounds which consist of a btd, dppz, or [ReCl(CO)$_3$(dppz)] acceptor and a triarylamine donor with CN, H, or OMe substituents were studied. The electron-withdrawing CN substituent is shown to lower the energy of frontier molecular orbitals, while the electron-donating OMe substituent increases the energy, as demonstrated using ^{1}H NMR spectroscopy, electrochemistry, and DFT calculations. Unsurprisingly, the TAA-based HOMO is affected more significantly than the acceptor-based LUMO, although this is still affected to a certain degree; overall, the effect is to narrow the HOMO−LUMO band gap as the substituent becomes more electron donating (σ^+ becomes more negative). This is reflected in the electronic absorption spectra, for which there is a bathochromic shift in the broad low-energy CT band as the substituent becomes more electron donating; this behavior is observed for the three different acceptors, which also bathochromically shift going from btd to dppz to [ReCl(CO)$_3$(dppz)]. TD-DFT calculations successfully predict these trends and predict the lowest energy absorption band to be predominantly ILCT in nature. Resonance Raman spectroscopy supports this assignment, indicating the substituent does not alter the electronic nature, only the orbital energy. CT emission bands show a similar trend in λ_{em} to the CT absorption bands and combined with the solvatochromism of emission inherent to such systems span the entire visible region. Substituents appear to have little effect on the change in dipole moment between ground and excited states or on the lifetime of a ^{3}ILCT dark state observed through transient absorption spectroscopy.

EXPERIMENTAL SECTION

General Experimental. btd-Br[62] and 1,10-phenanthroline-5,6-dione[63] were prepared using literature procedures. Commercially available reagents and solvents were used as received. Spectroscopic- or HPLC-grade solvents were used for all spectroscopic measure-

DOI: 10.1021/acs.inorgchem.6b01039
Inorg. Chem. XXXX, XXX, XXX−XXX

ments. Spectral data was analyzed using GRAMS A/I (ThermoScientific) and OriginPro v9.0 (Origin Lab Corp.). Compound numbering schemes are shown in Figure 1.

Materials. *5-(4-Trimethylsilylphenyl)benzo[c][1,2,5]thiadiazole.* A mixture of btd-Br (0.510 g, 2.37 mmol), 4-trimethylsilylphenylboronic acid (0.524 g, 2.70 mmol), and K_2CO_3 (1.80 g, 13.0 mmol) in toluene (15 mL), water (10 mL), and EtOH (5 mL) was bubbled with argon for 15 min. $PdCl_2$(dppf) (0.138 g, 0.168 mmol) was added and the reaction mixture heated at reflux overnight under an argon atmosphere. The reaction mixture was allowed to cool to rt, and the product was extracted into CH_2Cl_2 and washed with aq. NH_4Cl (satd) and then water. The organic extract was dried over $MgSO_4$, and the solvent was removed under reduced pressure. The residue was purified using preparative column chromatography (SiO_2, CH_2Cl_2) to afford 5-(4-trimethylsilylphenyl)benzo[*c*][1,2,5]thiadiazole (0.584 g, 87%) as a white crystalline solid. ^{1}H NMR (500 MHz, $CDCl_3$): δ 8.18 (dd, J = 1.7, 0.8 Hz, 1H, H_4), 8.05 (dd, J = 9.1, 0.7 Hz, 1H, H_7), 7.89 (dd, J = 9.1, 1.7 Hz, 1H, H_6), 7.71 (d, J = 8.3 Hz, 2H, $H_{2'}$), 7.68 (d, J = 8.3 Hz, 2H, $H_{3'}$), 0.35 (s, 9H, SiMe_3) ppm. ^{13}C NMR (126 MHz, $CDCl_3$): δ 155.52 (C_{3a}), 154.36 (C_{7a}), 142.53 (C_5), 140.98 ($C_{4'}$), 139.95 ($C_{1'}$), 134.21 ($C_{3'}$), 130.22 (C_6), 126.87 ($C_{2'}$), 121.60 (C_7), 118.65 (C_4), −1.00 (SiMe_3) ppm. HRMS (ESI) calcd for $C_{15}H_{17}N_2SSi$ ([M + H]$^+$): m/z 285.088. Found: m/z 285.088. Anal. Calcd for $C_{15}H_{16}N_2SSi$: C, 63.34; H, 5.67; N, 9.85. Found: C, 63.34; H, 5.65; N, 9.86.

5-(4-Iodophenyl)benzo[c][1,2,5]thiadiazole. A solution of 5-(4-trimethylsilylphenyl)benzo[*c*][1,2,5]thiadiazole (1.00 g, 3.52 mmol) in CH_2Cl_2 (100 mL) under an argon atmosphere was cooled to −78 °C using a dry ice/acetone bath. ICl (5.3 mL, 1 M in CH_2Cl_2) was added dropwise and the resultant mixture stirred at −78 °C under an argon atmosphere for 2 h. The dry ice/acetone bath was removed, excess ICl quenched by dropwise addition of aqueous $Na_2S_2O_5$ (satd, 20 mL), and the mixture allowed to warm to rt. The product was extracted into CH_2Cl_2 and washed with aqueous NH_4Cl (satd) and then water. The organic extract was dried over $MgSO_4$, and the solvent was removed under reduced pressure. The residue was purified using preparative column chromatography (SiO_2, CH_2Cl_2) to afford 5-(4-iodophenyl)-benzo[*c*][1,2,5]thiadiazole (1.07 g, 89%) as a white solid. ^{1}H NMR (500 MHz, $CDCl_3$): δ 8.12 (dd, J = 1.7, 0.7 Hz, 1H, H_4), 8.04 (dd, J = 9.1, 0.6 Hz, 1H, H_7), 7.82 (d, J = 8.5 Hz, 2H, $H_{3'}$), 7.80 (dd, J = 9.1, 1.8 Hz, 1H, H_6), 7.41 (d, J = 8.5 Hz, 2H, $H_{2'}$) ppm. ^{13}C NMR (126 MHz, $CDCl_3$): δ 155.38 (C_{3a}), 154.37 (C_{7a}), 141.41 (C_5), 139.16 ($C_{1'}$), 138.32 ($C_{3'}$), 129.70 (C_6), 129.31 ($C_{2'}$), 121.86 (C_7), 118.65 (C_4), 94.60 ($C_{4'}$) ppm. MS (MALDI-TOF) calcd for $C_{12}H_7IN_2S$ ([M]$^+$): m/z 337.94. Found: m/z 337.93. Anal. Calcd for $C_{12}H_7IN_2S$: C, 42.62; H, 2.09; N, 8.28. Found: C, 42.98; H, 1.90; N, 8.14.

5-(4-Di(4-methoxyphenyl)aminophenyl)benzo[c][1,2,5]-thiadiazole (btd-dmpab). A mixture of 5-(4-iodophenyl)benzo[*c*]-[1,2,5]thiadiazole (0.410 g, 1.21 mmol), di(4-methoxyphenyl)amine (0.426 g, 1.86 mmol), and ^{t}BuOK (0.475 g, 4.23 mmol) in toluene (30 mL) was bubbled with argon for 15 min. [^{t}Bu$_3$PH]BF_4 (0.050 g, 0.172 mmol) and $Pd_2(dba)_3$ (0.101 g, 0.110 mmol) were added, and the reaction mixture was heated at reflux overnight under an argon atmosphere. The reaction mixture was allowed to cool to rt, and the product was extracted into $CHCl_3$ and washed with aq. NH_4Cl (satd) and then water. The organic extract was dried over $MgSO_4$, and the solvent was removed under reduced pressure. The residue was purified using preparative column chromatography (basic Al_2O_3, CH_2Cl_2) to afford btd-dmpab (0.324 g, 61%) as an orange low-melting solid. ^{1}H NMR (500 MHz, $CDCl_3$): δ 8.09 (dd, J = 1.7, 0.7 Hz, 1H, H_4), 8.00 (dd, J = 9.2, 0.7 Hz, 1H, H_7), 7.87 (dd, J = 9.2, 1.8 Hz, 1H, H_6), 7.53 (d, J = 8.8 Hz, 2H, $H_{2'}$), 7.13 (d, J = 9.0 Hz, 4H, $H_{2''}$), 7.02 (d, J = 8.8 Hz, 2H, $H_{3'}$), 6.87 (d, J = 9.0 Hz, 4H, $H_{3''}$), 3.82 (s, 6H, OMe) ppm. ^{13}C NMR (126 MHz, $CDCl_3$): δ 156.41 ($C_{4''}$), 155.81 (C_{3a}), 154.12 (C_{7a}), 149.36 ($C_{4'}$), 142.22 (C_5), 140.51 ($C_{1''}$), 130.67 ($C_{1'}$), 130.13 (C_6), 128.08 ($C_{2'}$), 127.16 ($C_{2''}$), 121.38 (C_7), 120.16 ($C_{3'}$), 116.98 (C_4), 114.97 ($C_{3''}$), 55.64 (OMe) ppm. MS (MALDI-TOF) calcd for $C_{26}H_{21}N_3O_2S$ ([M]$^+$): m/z 439.14. Found: m/z 439.13. Anal. Calcd for $C_{26}H_{21}N_3O_2S$: C, 71.05; H, 4.82; N, 9.56. Found: C, 71.21; H, 4.69; N, 9.83.

5-(4-Diphenylaminophenyl)benzo[c][1,2,5]thiadiazole (btd-dpab). A mixture of btd-Br (0.516 g, 2.40 mmol), 4-diphenylaminophenylboronic acid (0.890 g, 3.08 mmol), and K_2CO_3 (1.84 g, 13.3 mmol) in toluene (15 mL), H_2O (10 mL), and EtOH (5 mL) was bubbled with argon for 15 min. $PdCl_2$(dppf) (0.100 g, 0.122 mmol) was added, and the reaction mixture was heated at reflux overnight under an argon atmosphere. The reaction mixture was allowed to cool, and the product was extracted into $CHCl_3$ and washed with NH_4Cl solution (satd) and then water. The organic extract was dried over $MgSO_4$, and the solvent was removed under reduced pressure. The residue was purified using preparative column chromatography (SiO_2, CH_2Cl_2) to afford btd-dpab (0.856 g, 94%) as a yellow crystalline solid. ^{1}H NMR (500 MHz, $CDCl_3$): δ 8.13 (dd, J = 1.7, 0.7 Hz, 1H, H_4), 8.03 (dd, J = 9.2, 0.7 Hz, 1H, H_7), 7.89 (dd, J = 9.2, 1.8 Hz, 1H, H_6), 7.59 (d, J = 8.7 Hz, 2H, $H_{2'}$), 7.30 (dd, J = 8.5, 7.4 Hz, 4H, $H_{3''}$), 7.18 (d, J = 8.7 Hz, 2H, $H_{3'}$), 7.17 (dd, J = 8.5, 1.0 Hz, 4H, $H_{2''}$), 7.08 (tt, J = 7.4, 1.1 Hz, 2H, $H_{4''}$) ppm. ^{13}C NMR (126 MHz, $CDCl_3$): δ 155.72 (C_{3a}), 154.20 (C_{7a}), 148.47 ($C_{4'}$), 147.49 ($C_{1''}$), 142.05 (C_5), 132.79 ($C_{1'}$), 130.10 (C_6), 129.55 ($C_{3''}$), 128.29 ($C_{2'}$), 125.02 ($C_{2''}$), 123.60 ($C_{4''}$), 123.35 ($C_{3'}$), 121.49 (C_7), 117.50 (C_4) ppm. HRMS (ESI) calcd for $C_{24}H_{18}N_3S$ ([M + H]$^+$): m/z 380.122. Found: m/z 380.121. Anal. Calcd for $C_{24}H_{17}N_3S$: C, 75.69; H, 4.52; N, 11.07. Found: C, 75.66; H, 4.37; N, 11.02.

5-(4-Di(4-iodophenyl)aminophenyl)benzo[c][1,2,5]thiadiazole. A mixture of btd-dpab (0.881 g, 2.32 mmol), KI (0.786 g, 4.73 mmol), and KIO_3 (0.511 g, 2.39 mmol) in AcOH (70 mL) and water (10 mL) was heated at 80 °C overnight. The reaction mixture was allowed to cool, and water was added. The resultant precipitate was filtered and washed with water. The residue was purified using preparative column chromatography (SiO_2, 10% EtOAc in $CHCl_3$) to afford 5-(4-di(4-iodophenyl)aminophenyl)benzo[*c*][1,2,5]thiadiazole (1.37 g, 93%) as a yellow solid. ^{1}H NMR (500 MHz, $CDCl_3$): δ 8.13 (dd, J = 1.8, 0.8 Hz, 1H, H_4), 8.05 (dd, J = 9.2, 0.8 Hz, 1H, H_7), 7.87 (dd, J = 9.2, 1.8 Hz, 1H, H_6), 7.60 (d, J = 8.8 Hz, 2H, $H_{2'}$), 7.58 (d, J = 8.9 Hz, 4H, $H_{3''}$), 7.17 (d, J = 8.7 Hz, 2H, $H_{3'}$), 6.89 (d, J = 8.9 Hz, 4H, $H_{2''}$) ppm. ^{13}C NMR (126 MHz, $CDCl_3$): δ 155.65 (C_{3a}), 154.29 (C_{7a}), 147.27 ($C_{4'}$), 146.88 ($C_{1''}$), 141.76 (C_5), 138.65 ($C_{3''}$), 134.37 ($C_{1'}$), 130.01 (C_6), 128.64 ($C_{2'}$), 126.47 ($C_{2''}$), 124.39 ($C_{3'}$), 121.67 (C_7), 117.92 (C_4), 86.80 ($C_{4''}$) ppm. MS (MALDI-TOF) calcd for $C_{24}H_{15}I_2N_3S$ ([M]$^+$): m/z 630.91. Found: m/z 630.88. Anal. Calcd for $C_{24}H_{15}I_2N_3S$: C, 45.66; H, 2.40; N, 6.66. Found: C, 45.51; H, 2.43; N, 6.55.

5-(4-Di(4-cyanophenyl)aminophenyl)benzo[c][1,2,5]thiadiazole (btd-dcpab). A solution of 5-(4-di(4-iodophenyl)aminophenyl)benzo-[*c*][1,2,5]thiadiazole (1.37 g, 2.17 mmol) in DMF (100 mL) was bubbled with argon for 15 min. CuCN (1.69 g, 18.9 mmol) was added, and the reaction mixture was heated at reflux overnight under an argon atmosphere. The reaction mixture was allowed to cool, and water was added. The resultant precipitate was filtered and washed with water. The residue was purified using preparative column chromatography (SiO_2, 20% CH_3CN in $CHCl_3$) to afford btd-dcpab (0.782 g, 84%) as a yellow solid. ^{1}H NMR (500 MHz, $CDCl_3$): δ 8.17 (dd, J = 1.7, 0.7 Hz, 1H, H_4), 8.08 (dd, J = 9.1, 0.6 Hz, 1H, H_7), 7.87 (dd, J = 9.1, 1.7 Hz, 1H, H_6), 7.72 (d, J = 8.6 Hz, 2H, $H_{2'}$), 7.57 (d, J = 8.8 Hz, 4H, $H_{3''}$), 7.26 (d, J = 8.6 Hz, 2H, $H_{3'}$), 7.19 (d, J = 8.8 Hz, 4H, $H_{2''}$) ppm. ^{13}C NMR (126 MHz, $CDCl_3$): δ 155.44 (C_{3a}), 154.36 (C_{7a}), 150.08 ($C_{1''}$), 145.44 ($C_{4'}$), 141.17 (C_5), 137.36 ($C_{1'}$), 133.80 ($C_{3''}$), 129.76 (C_6), 129.35 ($C_{2'}$), 127.00 ($C_{3'}$), 123.48 ($C_{2''}$), 121.90 (C_7), 118.87 (*CN*), 118.58 (C_4), 106.51 ($C_{4''}$) ppm. MS (MALDI-TOF) calcd for $C_{26}H_{15}N_5S$ ([M]$^+$): m/z 429.10. Found: m/z 429.08. Anal. Calcd for $C_{26}H_{15}N_5S$: C, 72.71; H, 3.52; N, 16.31. Found: C, 72.66; H, 3.81; N, 15.94.

11-(4-Diphenylaminophenyl)dipyrido[3,2-a:2′,3′-c]phenazine (dppz-dpab). A mixture of btd-dpab (0.256 g, 0.675 mmol) and $LiAlH_4$ (0.273 g, 7.19 mmol) in dry THF (20 mL) was stirred at rt overnight under an argon atmosphere. The reaction mixture was cooled to 0 °C, then water (0.5 mL) was added dropwise, followed by NaOH (1 mL, 10%), then more water (1.5 mL). Solids were removed by filtration through Celite ($CHCl_3$), and the product was extracted into $CHCl_3$ and washed with water. The organic extract was dried over

DOI: 10.1021/acs.inorgchem.6b01039
Inorg. Chem. XXXX, XXX, XXX−XXX

$MgSO_4$, and the solvent was removed under reduced pressure. 1,10-Phenanthroline-5,6-dione (0.134 g, 0.638 mmol) and EtOH (150 mL) were then added, and the mixture was heated at reflux overnight. The reaction mixture was allowed to cool, and the solvent was removed under reduced pressure. The residue was purified using preparative column chromatography (SiO_2, 20% EtOAc in $CHCl_3$) to afford dppz-dpab (0.204 g, 39%) as an orange crystalline solid. ^{1}H NMR (500 MHz, $CDCl_3$): δ 9.64 (m, 2H, $H_{1,8}$), 9.28 (m, 2H, $H_{3,6}$), 8.50 (d, J = 1.9 Hz, 1H, H_{10}), 8.37 (d, J = 8.8 Hz, 1H, H_{13}), 8.20 (dd, J = 8.9, 2.1 Hz, 1H, H_{12}), 7.80 (m, 2H, $H_{2,7}$), 7.75 (d, J = 8.7 Hz, 2H, $H_{2'}$), 7.33 (dd, J = 8.5, 7.4 Hz, 4H, $H_{3''}$), 7.24 (d, J = 8.7 Hz, 2H, $H_{3'}$), 7.20 (d, J = 8.6, 1.1 Hz, 4H, $H_{2''}$), 7.10 (tt, J = 7.3, 1.2 Hz, 2H, $H_{4''}$) ppm. ^{13}C NMR (126 MHz, $CDCl_3$): δ 152.62 ($C_{3/6}$), 152.47 ($C_{3/6}$), 148.65 ($C_{4'}$), 148.40 ($C_{4a/4b}$), 148.00 ($C_{4a/4b}$), 147.49 ($C_{1''}$), 143.09 (C_{9a}), 142.93 (C_{11}), 141.95 (C_{13a}), 141.59 ($C_{8b/14a}$), 140.72 ($C_{8b/14a}$), 133.97 ($C_{1/8}$), 133.89 ($C_{1/8}$), 132.64 ($C_{1'}$), 130.48 (C_{12}), 129.90 (C_{13}), 129.60 ($C_{3''}$), 128.41 ($C_{2'}$), 127.89 ($C_{8a/14b}$), 127.80 ($C_{8a/14b}$), 125.46 (C_{10}), 125.13 ($C_{2''}$), 124.32 ($C_{2/7}$), 124.30 ($C_{2/7}$), 123.71 ($C_{4''}$), 123.36 ($C_{3'}$) ppm. HRMS (ESI) calcd for $C_{36}H_{24}N_5$ ($[M + H]^+$): m/z 526.203. Found: m/z 526.204. Anal. Calcd for $C_{36}H_{23}N_5{\cdot}CHCl_3$: C, 68.90; H, 3.75; N, 10.86. Found: C, 69.01; H, 3.71; N, 10.93.

11-(4-Di(4-methoxyphenyl)aminophenyl)dipyrido[3,2-a:2′,3′-c]-phenazine (dppz-dmpab). A mixture of btd-dmpab (0.720 g, 1.64 mmol) and $LiAlH_4$ (0.621 g, 16.4 mmol) in dry THF (20 mL) was stirred at rt overnight under an argon atmosphere. The reaction mixture was cooled to 0 °C using an ice bath and excess $LiAlH_4$ quenched by dropwise addition of water (0.5 mL), aqueous NaOH (0.5 mL, 15%), and more water (1.5 mL). Solids were removed by filtration through Celite ($CHCl_3$), and the product was extracted into $CHCl_3$ and washed with water. The organic extract was dried over $MgSO_4$, and the solvent was removed under reduced pressure. 1,10-Phenanthroline-5,6-dione (0.346 g, 1.65 mmol) and EtOH (200 mL) were added, and the mixture was heated at reflux overnight. The reaction mixture was allowed to cool to rt, and the resultant precipitate was filtered and washed with EtOH. The residue was purified using preparative column chromatography (basic Al_2O_3, 1% MeOH in $CHCl_3$) to afford dppz-dmpab (0.309 g, 32%) as a red solid. ^{1}H NMR (500 MHz, $CDCl_3$): δ 9.56 (m, 2H, $H_{1,8}$), 9.23 (m, 2H, $H_{3,6}$), 8.40 (d, J = 1.9 Hz, 1H, H_{10}), 8.27 (d, J = 8.9 Hz, 1H, H_{13}), 8.14 (dd, J = 8.9, 2.0 Hz, 1H, H_{12}), 7.74 (m, 2H, $H_{2,7}$), 7.68 (d, J = 8.7 Hz, 2H, $H_{2'}$), 7.16 (d, J = 8.9 Hz, 4H, $H_{2''}$), 7.07 (d, J = 8.7 Hz, 2H, $H_{3'}$), 6.89 (d, J = 8.9 Hz, 4H, $H_{3''}$), 3.83 (s, 6H, O*Me*) ppm. ^{13}C NMR (126 MHz, $CDCl_3$): δ 156.47 ($C_{4''}$), 152.56 ($C_{3/6}$), 152.39 ($C_{3/6}$), 149.49 ($C_{4'}$), 148.50 ($C_{4a/4b}$), 148.29 ($C_{4a/4b}$), 143.06 (C_{9a}), 142.97 (C_{11}), 141.77 (C_{13a}), 141.45 ($C_{8b/14a}$), 140.48 ($C_{1''}$), 140.46 ($C_{8b/14a}$), 133.78 ($C_{1/8}$), 133.66 ($C_{1/8}$), 130.51 ($C_{1'}$), 130.34 (C_{12}), 129.73 (C_{13}), 128.18 ($C_{2'}$), 127.80 ($C_{8a/14b}$), 127.69 ($C_{8a/14b}$), 127.23 ($C_{2''}$), 124.84 (C_{10}), 124.18 ($C_{2/7}$), 124.15 ($C_{2/7}$), 120.17 ($C_{3'}$), 115.00 ($C_{3''}$), 55.66 (O*Me*) ppm. HRMS (ESI) calcd for $C_{38}H_{28}N_5O_2$ ($[M + H]^+$): m/z 586.224. Found: m/z 586.219. Anal. Calcd for $C_{38}H_{27}N_5O_2{\cdot}CHCl_3$: C, 66.44; H, 4.00; N, 9.93. Found: C, 66.45; H, 3.97; N, 10.01.

11-(4-Di(4-cyanophenyl)aminophenyl)dipyrido[3,2-a:2′,3′-c]-phenazine (dppz-dcpab). A mixture of btd-dcpab (0.683 g, 1.59 mmol), $CoCl_2$ (0.052 g, 0.401 mmol), and $NaBH_4$ (0.538 g, 14.2 mmol) in EtOH (200 mL) was heated at reflux overnight under an argon atmosphere. The solvent was removed under reduced pressure, and the resultant precipitate was extracted into $CHCl_3$ and washed with aqueous NH_4Cl (satd) and water. The organic extract was dried over $MgSO_4$, and the solvent was removed under reduced pressure. 1,10-Phenanthroline-5,6-dione (0.299 g, 1.42 mmol) and EtOH (200 mL) were added, and the mixture was heated at reflux overnight. The reaction mixture was allowed to cool to rt, and the resultant precipitate was filtered and washed with EtOH to afford dppz-dcpab (0.337 g, 41%) as a red solid. ^{1}H NMR (500 MHz, $CDCl_3$): δ 9.67 (m, 2H, $H_{1,8}$), 9.29 (m, 2H, $H_{3,6}$), 8.57 (dd, J = 2.0, 0.4 Hz, 1H, H_{10}), 8.45 (dd, J = 8.9, 0.4 Hz, 1H, H_{13}), 8.20 (dd, J = 8.9, 2.1 Hz, 1H, H_{12}), 7.89 (d, J = 8.7 Hz, 2H, $H_{2'}$), 7.82 (m, 2H, $H_{2,7}$), 7.60 (d, J = 8.9 Hz, 4H, $H_{3''}$), 7.32 (d, J = 8.6 Hz, 2H, $H_{3'}$), 7.22 (d, J = 8.9 Hz, 4H, $H_{2''}$) ppm. ^{13}C NMR (126 MHz, $CDCl_3$): δ 152.90 ($C_{3/6}$), 152.82 ($C_{3/6}$), 150.15 ($C_{1''}$), 148.71 ($C_{4a/4b}$), 148.59 ($C_{4a/4b}$), 145.61 ($C_{4'}$), 142.86 (C_{9a}), 142.15 (C_{13a}), 141.99 (C_{11}), 141.95 ($C_{8b/14a}$), 141.38 ($C_{8b/14a}$), 137.34 ($C_{1'}$), 133.93 ($C_{1/8}$), 133.91 ($C_{1/8}$), 133.88 ($C_{3''}$), 130.32 (C_{13}), 130.22 (C_{12}), 129.50 ($C_{2'}$), 127.75 ($C_{8a/14b}$), 127.66 ($C_{8a/14b}$), 127.09 ($C_{3'}$), 126.67 (C_{10}), 124.39 ($C_{2/7}$), 124.36 ($C_{2/7}$), 123.58 ($C_{2''}$), 118.91 (*CN*), 106.64 ($C_{4''}$) ppm. HRMS (ESI) calcd for $C_{38}H_{22}N_7$ ($[M + H]^+$): m/z 576.193. Found: m/z 576.189. Anal. Calcd for $C_{38}H_{21}N_7{\cdot}H_2O$: C, 76.88; H, 3.91; N, 16.52. Found: C, 76.56; H, 3.87; N, 16.37.

fac-Chlorotricarbonyl(11-(4-diphenylaminophenyl)dipyrido[3,2-a:2′,3′-c]phenazine)rhenium(I) ([ReCl(CO)$_3$(dppz-dpab)]). A mixture of dppz-dpab (0.298 g, 0.568 mmol) and $[ReCl(CO)_5]$ (0.272 g, 0.751 mmol) in EtOH (100 mL) was heated at reflux overnight. The reaction mixture was allowed to cool, and the precipitate was filtered and washed with EtOH to afford $[ReCl(CO)_3(dppz\text{-}dpab)]$ (0.429 g, 91%) as a purple solid. ^{1}H NMR (500 MHz, $CDCl_3$): δ 9.81 (m, 2H, $H_{1,8}$), 9.45 (m, 2H, $H_{3,6}$), 8.53 (s, 1H, H_{10}), 8.42 (d, J = 8.9 Hz, 1H, H_{13}), 8.32 (d, J = 9.0 Hz, 1H, H_{12}), 8.00 (m, 2H, $H_{2,7}$), 7.76 (d, J = 8.4 Hz, 2H, $H_{2'}$), 7.34 (t, J = 7.7 Hz, 4H, $H_{3''}$), 7.25 (d, J = 8.6 Hz, 2H, $H_{3'}$), 7.21 (d, J = 7.9 Hz, 4H, $H_{2''}$), 7.13 (t, J = 7.4 Hz, 2H, $H_{4''}$) ppm. ^{13}C NMR (126 MHz, $CDCl_3$): δ 196.98 (CO_{eq}), 189.44 (CO_{ax}), 154.36 ($C_{3/6}$), 154.18 ($C_{3/6}$), 149.48 ($C_{4a/4b}$), 149.23 ($C_{4a/4b}$), 149.17 ($C_{4'}$), 147.30 ($C_{1''}$), 144.52 (C_{11}), 143.63 (C_{9a}), 142.41 (C_{13a}), 139.62 ($C_{8b/14a}$), 138.57 ($C_{8b/14a}$), 135.89 ($C_{1/8}$), 135.74 ($C_{1/8}$), 132.08 (C_{12}), 131.64 ($C_{1'}$), 130.81 ($C_{8a/14b}$), 130.71 ($C_{8a/14b}$), 130.14 (C_{13}), 129.67 ($C_{3''}$), 128.51 ($C_{2'}$), 127.01 ($C_{2/7}$), 126.97 ($C_{2/7}$), 125.36 ($C_{2''}$), 125.26 (C_{10}), 124.01 ($C_{4''}$), 122.97 ($C_{3'}$) ppm. HRMS (ESI) calcd for $C_{39}H_{23}ClN_5NaO_3Re$ ($[M + Na]^+$): m/z 854.094. Found: m/z 854.081. Anal. Calcd for $C_{39}H_{23}ClN_5O_3Re{\cdot}H_2O$: C, 55.15; H, 2.97; N, 8.25. Found: C, 54.89; H, 3.01; N, 8.23.

fac-Chlorotricarbonyl(11-(4-di(4-methoxyphenyl)aminophenyl)-dipyrido[3,2-a:2′,3′-c]phenazine)rhenium(I) ([ReCl(CO)$_3$(dppz-dmpab)]). A mixture of dppz-dmpab (0.068 g, 0.116 mmol) and $[ReCl(CO)_5]$ (0.049 g, 0.134 mmol) in EtOH (100 mL) was heated at reflux overnight. The reaction was allowed to cool to rt, and the resultant precipitate was filtered and washed with EtOH to afford $[ReCl(CO)_3(dppz\text{-}dmpab)]$ (0.080 g, 78%) as a dark red solid. ^{1}H NMR ($CDCl_3$): δ 9.78 (m, 2H, $H_{1,8}$), 9.44 (m, 2H, $H_{3,6}$), 8.47 (d, J = 1.5 Hz, 1H, H_{10}), 8.37 (d, J = 8.9 Hz, 1H, H_{13}), 8.29 (dd, J = 9.0, 1.9 Hz, 1H, H_{12}), 7.98 (m, 2H, $H_{2,7}$), 7.71 (d, J = 8.8 Hz, 2H, $H_{2'}$), 7.17 (d, J = 8.9 Hz, 4H, $H_{2''}$), 7.08 (d, J = 8.0 Hz, 2H, $H_{3'}$), 6.91 (d, J = 9.0 Hz, 4H, $H_{3''}$), 3.84 (s, 6H, O*Me*) ppm. ^{13}C NMR (126 MHz, $CDCl_3$): δ 196.85 (CO_{eq}), 189.32 (CO_{ax}), 156.55 ($C_{4''}$), 154.15 ($C_{3/6}$), 153.93 ($C_{3/6}$), 149.88 ($C_{4'}$), 149.30 ($C_{4a/4b}$), 149.00 ($C_{4a/4b}$), 144.54 (C_{11}), 143.59 (C_{9a}), 142.22 (C_{13a}), 140.05 ($C_{1''}$), 139.43 ($C_{8b/14a}$), 138.22 ($C_{8b/14a}$), 135.71 ($C_{1/8}$), 135.53 ($C_{1/8}$), 131.91 (C_{12}), 130.70 ($C_{8a/14b}$), 130.58 ($C_{8a/14b}$), 129.88 (C_{13}), 129.41 ($C_{1'}$), 128.20 ($C_{2'}$), 127.30 ($C_{2''}$), 126.81 ($C_{2/7}$), 126.76 ($C_{2/7}$), 124.49 (C_{10}), 119.70 ($C_{3'}$), 114.92 ($C_{3''}$), 55.53 (O*Me*) ppm. HRMS (ESI) calcd for $C_{41}H_{29}N_5O_6Re$ ($[M\text{-}Cl{+}H_2O]^+$): m/z 874.167. Found: m/z = 874.171. Anal. Calcd for $C_{41}H_{27}N_5ClO_5{\cdot}0.5H_2O$: C, 54.69; H, 3.13; N, 7.78. Found: C, 54.59; H, 3.16; N, 7.95.

fac-Chlorotricarbonyl(11-(4-di(4-cyanophenyl)aminophenyl)-dipyrido[3,2-a:2′,3′-c]phenazine)rhenium(I) ([ReCl(CO)$_3$(dppz-dcpab)]). A mixture of dppz-dcpab (0.050 g, 0.087 mmol) and $[ReCl(CO)_5]$ (0.038 g, 0.105 mmol) in EtOH (100 mL) was heated at reflux overnight. The reaction was allowed to cool to rt, and the resultant precipitate was filtered and washed with EtOH to afford $[ReCl(CO)_3(dppz\text{-}dcpab)]$ (0.039 g, 45%) as a dark yellow solid. ^{1}H NMR (500 MHz, $CDCl_3$): δ 9.86 (m, 2H, $H_{1,8}$), 9.47 (m, 2H, $H_{3,6}$), 8.62 (d, J = 2.0 Hz, 1H, H_{10}), 8.52 (d, J = 8.9 Hz, 1H, H_{13}), 8.32 (dd, J = 8.9, 2.1 Hz, 1H, H_{12}), 8.04 (m, 2H, $H_{2,7}$), 7.90 (d, J = 8.6 Hz, 2H, $H_{2'}$), 7.61 (d, J = 8.9 Hz, 4H, $H_{3''}$), 7.34 (d, J = 8.6 Hz, 2H, $H_{3'}$), 7.23 (d, J = 8.9 Hz, 4H, $H_{2''}$) ppm. ^{13}C NMR (126 MHz, $CDCl_3$): δ 196.90 (CO_{eq}), 189.38 (CO_{ax}), 154.58 ($C_{3/6}$), 154.47 ($C_{3/6}$), 150.07 ($C_{1''}$), 149.64 ($C_{4a/4b}$), 149.46 ($C_{4a/4b}$), 146.15 ($C_{4'}$), 143.64 (C_{9a}), 143.38 (C_{13a}), 142.60 (C_{11}), 139.93 ($C_{8b/14a}$), 139.25 ($C_{8b/14a}$), 136.53 ($C_{1/8}$), 135.87 ($C_{1/8,1'}$), 133.93 ($C_{3''}$), 131.88 (C_{13}), 130.72 (C_{12}), 130.64 ($C_{8a/14b}$), 130.58 ($C_{8a/14b}$), 129.58 ($C_{2'}$), 127.11 ($C_{2/7}$), 127.08 ($C_{2/7}$), 126.99 ($C_{3'}$), 126.66 (C_{10}), 123.74 ($C_{2''}$), 118.84 (CN), 106.87 ($C_{4''}$) ppm. HRMS (ESI) calcd for $C_{41}H_{23}N_7O_4Re$ ($[M\text{-}Cl{+}H_2O]^+$): m/z

DOI: 10.1021/acs.inorgchem.6b01039
Inorg. Chem. XXXX, XXX, XXX−XXX

864.136. Found: m/z 864.134. Anal. Calcd for $C_{41}H_{21}ClN_7O_3Re$: C, 55.88; H, 2.40; N, 11.13. Found: C, 55.72; H, 2.30; N, 11.35.

Physical Measurements. ^{1}H NMR spectra were recorded at 500 MHz and ^{13}C at 126 MHz on a Varian 500AR spectrometer. All samples were recorded at 25 °C in 5 mm diameter tubes. Chemical shifts were referenced internally to residual nonperdeuterated solvent using δ values as reported by Gottlieb et al.[64] Coupling constants are rounded to the nearest 0.1 Hz. Assignment of signals is assisted through the use of 2D NMR techniques (COSY, NOESY, ^{1}H−^{13}C HSQC, and ^{1}H−^{13}C HMBC), recorded on a Varian 500AR spectrometer using standard pulse sequences. HR-ESI-MS was performed on a Bruker MicrOTOF-Q mass spectrometer operating in positive mode. Values are quoted as m/z ratio, with an instrumental uncertainty of $m/z \pm 0.003$. MALDI-TOF MS was performed on an Applied Biosystems 4800 Tandem TOF mass spectrometer calibrated externally over the range m/z 300−3500. The analyte was mechanically blended with the matrix (TCNQ) using a mixer mill and applied as a suspension to the sample plate. Values are reported as m/z values, with an instrumental uncertainty of $m/z \pm 0.08$. Analysis of elemental composition was made by the Campbell Microanalytical Laboratory at the University of Otago using a Carlo Erba 1108 CHNS combustion analyzer. The estimated error is the measurements in ±0.4%.

For X-ray crystallography, single crystals were attached with Paratone N to a fiber loop supported in a copper mounting pin and then quenched in a cold nitrogen stream. Data were collected at 100 K using Cu Kα radiation (microsource, mirror monochromated) using an Agilent Supernova diffractometer with an Atlas detector. Data processing was undertaken with CrysAlisPro.[65] A multiscan or face-indexed absorption correction was applied to the data. Structures were solved by direct methods with SHELXS-97 and extended and refined with SHELXL-97 using the X-Seed interface.[66,67] The non-hydrogen atoms in the asymmetric unit were modeled with anisotropic displacement parameters, and a riding atom model with group displacement parameters was used for the hydrogen atoms. X-ray crystallographic data is available in CIF format (Supporting Information). CCDC 1435218 and 1475303 contain the supplementary crystallographic data for this article. These data can be obtained free of charge from The Cambridge Crystallographic Data Centre via www.ccdc.cam.ac.uk/data_request/cif.

Crystal Data for dppz-dmpab·CHCl$_3$. $C_{39}H_{28}Cl_3N_5O_2$, M = 705.01, orange plate, 0.62 × 0.11 × 0.03 mm^3, triclinic, a = 5.9904(1) Å, b = 10.3974(3) Å, c = 27.3036(6) Å, α = 92.437(2)°, β = 96.088(2)°, γ = 100.467(2)°, V = 1659.54(7) Å^3, space group P-1 (#2), Z = 2, μ(Cu Kα) = 2.858 mm^{-1}, $2\theta_{max}$ = 148.46°, 18 128 reflections measured, 6559 independent reflections (R_{int} = 0.0460). The final $R_1(F)$ = 0.0455 ($I > 2\sigma(I)$); 0.0491 (all data). The final $wR_2(F^2)$ = 0.1265 ($I > 2\sigma(I)$); 0.1311 (all data). GoF = 1.045. CCDC 1475303.

Crystal Data for 5-(4-trimethylsilylphenyl)benzo[c][1,2,5]-thiadiazole. $C_{15}H_{16}N_2SSi$, M = 284.45, colorless plate, 0.52 × 0.22 × 0.02 mm^3, triclinic, a = 7.4105(2) Å, b = 12.6297(4) Å, c = 17.1588(7) Å, α = 110.283(3)°, β = 94.904(3)°, γ = 99.001(3)°, V = 1470.78(9) Å^3, space group P-1 (#2), Z = 4, μ(Cu Kα) = 2.625 mm^{-1},$2\theta_{max}$ = 153.18°, 15 320 reflections measured, 6106 independent reflections (R_{int} = 0.0366). The final $R_1(F)$ = 0.0440 ($I > 2\sigma(I)$); 0.0484 (all data). The final $wR_2(F^2)$ = 0.1214 ($I > 2\sigma(I)$); 0.1269 (all data). GoF = 1.050. CCDC 1435218.

The electrochemical cell for cyclic voltammetry was made up of a 1 mm diameter platinum rod working electrode embedded in a KeL-F cylinder with a platinum auxiliary electrode and a Ag/AgCl reference electrode. The potential of the cell was controlled by an ADI Powerlab 4SP potentiostat. Solutions were typically about 10^{-3} M in CH_2Cl_2 with 0.1 M tetrabutylammonium hexafluorophosphate (NBu_4PF_6) as a supporting electrolyte and were purged with argon for approximately 5 min prior to measurement. The scanning rate was 100 mV s^{-1}, and the cyclic voltammograms were calibrated against the decamethylferrocenium/decamethylferrocene (Fc^{*+}/Fc^*) couple (−0.012 V in CH_2Cl_2) and are reported relative to the saturated calomel electrode (SCE) for comparison with other data by subtracting 0.045 V.[68]

Steady-state absorption spectra were recorded as solutions on a PerkinElmer Lambda 950 UV/vis/NIR Spectrometer. Extinction coefficients were obtained from serial dilution measurements.

Steady-state emission spectra were recorded on a Princeton Instruments SP2150i spectrograph with a 300 grooves mm^{-1} grating and a Pixis 100B CCD and controlled using Winspec/32 v2.6.80 software using 355 nm excitation from a Cobalt Zouk solid state diode laser.

FT-Raman spectra were collected on powder samples using a Bruker IFS-55 interferometer with an FRA/106S attachment. The excitation source was a Nd:YAG laser with an excitation wavelength of 1064 nm. Raman photons were detected with a liquid nitrogen-cooled D418T germanium diode. Spectra were measured with 256 scans, with a laser power of 100 mW and spectral resolution of 4 cm^{-1}.

Resonance Raman spectra were recorded using a previously described setup.[69−72] Excitation wavelengths 351, 406, and 413 nm were provided by an I-302 krypton ion laser (Coherent Inc.), 457, 488, and 514 nm were provided by an Innova Sabre argon ion laser (Coherent Inc.), and 448 and 532 nm were provided by crystal diode lasers (CrystaLaser). Concentrations were typically 1 mM in CH_2Cl_2.

Transient absorption and emission spectra were recorded on CH_2Cl_2 solutions with concentrations typically 1 × 10^{-5} M, which were bubbled with argon for 10 min prior to measurement. Transients were acquired using an LP920 K TA systems (Edinburgh Instruments), with excitation at 355 nm from pulsed third-harmonic radiation from a Brilliant (Quantel) Nd:YAG laser at 1 Hz, and a Xe900 450 W xenon arc lamp controlled by an XP920 pulser as the probe source in TA mode. Photons were dispersed using a TMS300-A Czerney-Turner monochromator with 1800 grooves mm^{-1} grating, recorded on a R928 (Hamamatsu) photomultiplier, and transcribed on a TDS3012C (Tektronix) digital oscilloscope.

Calculations were performed using the Gaussian09 package. Geometry optimization and harmonic vibrational frequency calculations were performed in vacuo using density functional theory (DFT) employing the B3LYP functional.[73−75] A LANL2DZ effective core potential and associated basis set was used for the rhenium atoms,[76−78] while the 6-31G(d) basis set was used for all other atoms.[79,80] Time-dependent density functional theory (TD-DFT) calculations using the CAM-B3LYP functional[81] were run both in vacuo and with a SCRF solvent field.[82−85] Calculated vibrational spectra were generated using GaussSum v2.2.5 software[86] and scaled to give the lowest value for the mean absolute deviation for band position from experimental data, with scale factors typically around 0.975. Raman activities calculated by G09 were converted to Raman scattering cross sections using an intensity correction.[87] Vibrational modes were illustrated using Molden.[88]

■ ASSOCIATED CONTENT

Supporting Information

The Supporting Information is available free of charge on the ACS Publications website at DOI: 10.1021/acs.inorgchem.6b01039.

Tabulated ^{1}H NMR data, experimental vs calculated FT-Raman spectra, tabulated mean absolute deviations, tabulated Raman vibrational modes, tabulated electrochemical data, DFT-predicted frontier molecular orbitals, tabulated TD-DFT data, calculated emission energies, resonance-enhanced vibrational mode representations, emission spectra, and Lippert−Mataga plots, and crystal structure plot (PDF)

Crystallographic data in CIF format (CCDC 1435218, 1475303) (CIF)

■ AUTHOR INFORMATION

Corresponding Authors

*E-mail: nlucas@chemistry.otago.ac.nz. Phone: +64 3 479 5377. Fax: +64 3 479 7906.

DOI: 10.1021/acs.inorgchem.6b01039
Inorg. Chem. XXXX, XXX, XXX−XXX

*E-mail: kgordon@chemistry.otago.ac.nz. Phone: +64 3 479 7599. Fax: +64 3 479 7906.

Author Contributions

†C.B.L. and H.v.d.S. contributed equally.

Funding

The authors would like to acknowledge the MacDiarmid Institute for Advanced Materials and Nanotechnology for funding.

Notes

The authors declare no competing financial interest.

REFERENCES

(1) Neto, B. A. D.; Lapis, A. A. M.; da Silva Júnior, E. N.; Dupont, J. *Eur. J. Org. Chem.* **2013**, *2013*, 228.
(2) Wu, Y.; Zhu, W. *Chem. Soc. Rev.* **2013**, *42*, 2039.
(3) Gautam, P.; Misra, R.; Siddiqui, S. A.; Sharma, G. D. *ACS Appl. Mater. Interfaces* **2015**, *7*, 10283.
(4) Hagfeldt, A.; Boschloo, G.; Sun, L.; Kloo, L.; Pettersson, H. *Chem. Rev.* **2010**, *110*, 6595.
(5) Sun, L.; Bai, F.-Q.; Zhao, Z.-X.; Zhang, H.-X. *Sol. Energy Mater. Sol. Cells* **2011**, *95*, 1800.
(6) Berezin, M. Y.; Achilefu, S. *Chem. Rev.* **2010**, *110*, 2641.
(7) Caruso, F.; Atalla, V.; Ren, X.; Rubio, A.; Scheffler, M.; Rinke, P. *Phys. Rev. B: Condens. Matter Mater. Phys.* **2014**, *90*, 085141.
(8) Keller, S. N.; Veltri, N. L.; Sutherland, T. C. *Org. Lett.* **2013**, *15*, 4798.
(9) Larsen, C. B.; van der Salm, H.; Clark, C. A.; Elliott, A. B. S.; Fraser, M. G.; Horvath, R.; Lucas, N. T.; Sun, X.-Z.; George, M. W.; Gordon, K. C. *Inorg. Chem.* **2014**, *53*, 1339.
(10) Amacher, A.; Luo, H.; Liu, Z.; Bircher, M.; Cascella, M.; Hauser, J.; Decurtins, S.; Zhang, D.; Liu, S.-X. *RSC Adv.* **2014**, *4*, 2873.
(11) Sato, S.; Hashimoto, K.; Tajima, K. *Synth. Met.* **2011**, *161*, 1289.
(12) Leriche, P.; Frère, P.; Cravino, A.; Alévêque, O.; Roncali, J. *J. Org. Chem.* **2007**, *72*, 8332.
(13) Marszalek, M.; Nagane, S.; Ichake, A.; Humphry-Baker, R.; Paul, V.; Zakeeruddin, S. M.; Gratzel, M. *J. Mater. Chem.* **2012**, *22*, 889.
(14) Qin, C.; Fu, Y.; Chui, C.-H.; Kan, C.-W.; Xie, Z.; Wang, L.; Wong, W.-Y. *Macromol. Rapid Commun.* **2011**, *32*, 1472.
(15) Yang, Y.; Farley, R. T.; Steckler, T. T.; Eom, S.-H.; Reynolds, J. R.; Schanze, K. S.; Xue, J. *Appl. Phys. Lett.* **2008**, *93*, 163305.
(16) Dhar, J.; Swathi, K.; Karothu, D. P.; Narayan, K. S.; Patil, S. *ACS Appl. Mater. Interfaces* **2015**, *7*, 670.
(17) Qian, G.; Dai, B.; Luo, M.; Yu, D.; Zhan, J.; Zhang, Z.; Ma, D.; Wang, Z. Y. *Chem. Mater.* **2008**, *20*, 6208.
(18) Lu, X.; Fan, S.; Wu, J.; Jia, X.; Wang, Z.-S.; Zhou, G. *J. Org. Chem.* **2014**, *79*, 6480.
(19) Moss, K. C.; Bourdakos, K. N.; Bhalla, V.; Kamtekar, K. T.; Bryce, M. R.; Fox, M. A.; Vaughan, H. L.; Dias, F. B.; Monkman, A. P. *J. Org. Chem.* **2010**, *75*, 6771.
(20) Li, Y.; Ren, T.; Dong, W.-J. *J. Photochem. Photobiol., A* **2013**, *251*, 1.
(21) Qin, C.; Islam, A.; Han, L. *Dyes Pigm.* **2012**, *94*, 553.
(22) Fraser, M. G.; Blackman, A. G.; Irwin, G. I. S.; Easton, C. P.; Gordon, K. C. *Inorg. Chem.* **2010**, *49*, 5180.
(23) Fraser, M. G.; van der Salm, H.; Cameron, S. A.; Barnsley, J. E.; Gordon, K. C. *Polyhedron* **2013**, *52*, 623.
(24) Goze, C.; Leiggener, C.; Liu, S.-X.; Sanguinet, L.; Levillain, E.; Hauser, A.; Decurtins, S. *ChemPhysChem* **2007**, *8*, 1504.
(25) Hino, J. K.; Della Ciana, L.; Dressick, W. J.; Sullivan, B. P. *Inorg. Chem.* **1992**, *31*, 1072.
(26) Maestri, M.; Armaroli, N.; Balzani, V.; Constable, E. C.; Thompson, A. M. W. C. *Inorg. Chem.* **1995**, *34*, 2759.
(27) Pohl, R.; Anzenbacher, P. *Org. Lett.* **2003**, *5*, 2769.
(28) Pohl, R.; Montes, V. A.; Shinar, J.; Anzenbacher, P. *J. Org. Chem.* **2004**, *69*, 1723.
(29) Rillema, D. P.; Nagle, J. K.; Barringer, L. F.; Meyer, T. J. *J. Am. Chem. Soc.* **1981**, *103*, 56.
(30) Yamaguchi, Y.; Ochi, T.; Wakamiya, T.; Matsubara, Y.; Yoshida, Z.-i. *Org. Lett.* **2006**, *8*, 717.
(31) Zhao, C.-H.; Sakuda, E.; Wakamiya, A.; Yamaguchi, S. *Chem. - Eur. J.* **2009**, *15*, 10603.
(32) Lowry, T. H.; Richardson, K. S. 1981.
(33) van der Salm, H.; Larsen, C. B.; McLay, J. R. W.; Huff, G. S.; Gordon, K. C. *Inorg. Chim. Acta* **2015**, *428*, 1.
(34) van der Salm, H.; Larsen, C. B.; McLay, J. R. W.; Fraser, M. G.; Lucas, N. T.; Gordon, K. C. *Dalton Trans.* **2014**, *43*, 17775.
(35) Fraser, M. G.; van der Salm, H.; Cameron, S. A.; Barnsley, J. E.; Gordon, K. C. *Polyhedron* **2013**, *52*, 623.
(36) van der Salm, H.; Fraser, M. G.; Horvath, R.; Turner, J. O.; Greetham, G. M.; Clark, I. P.; Towrie, M.; Lucas, N. T.; George, M. W.; Gordon, K. C. *Inorg. Chem.* **2014**, *53*, 13049.
(37) Fraser, M. G.; Clark, C. A.; Horvath, R.; Lind, S. J.; Blackman, A. G.; Sun, X.-Z.; George, M. W.; Gordon, K. C. *Inorg. Chem.* **2011**, *50*, 6093.
(38) Echevarria, A.; Miller, J.; Nascimento, M. G. *Magn. Reson. Chem.* **1985**, *23*, 809.
(39) Solčániová, E.; Toma, S. *Org. Magn. Reson.* **1980**, *14*, 138.
(40) Kim, T. Y.; Elliott, A. B. S.; Shaffer, K. J.; John McAdam, C.; Gordon, K. C.; Crowley, J. D. *Polyhedron* **2013**, *52*, 1391.
(41) van der Salm, H.; Fraser, M. G.; Horvath, R.; Cameron, S. A.; Barnsley, J. E.; Sun, X.-Z.; George, M. W.; Gordon, K. C. *Inorg. Chem.* **2014**, *53*, 3126.
(42) Clark, J.; Archer, R.; Redding, T.; Foden, C.; Tant, J.; Geerts, Y.; Friend, R. H.; Silva, C. *J. Appl. Phys.* **2008**, *103*, 124510.
(43) Walsh, P. J.; Gordon, K. C.; Lundin, N. J.; Blackman, A. G. *J. Phys. Chem. A* **2005**, *109*, 5933.
(44) Li, Y.; Cao, Y.; Gao, J.; Wang, D.; Yu, G.; Heeger, A. J. *Synth. Met.* **1999**, *99*, 243.
(45) Easwaramoorthi, S.; Thamaraiselvi, P.; Duraimurugan, K.; Beneto, A. J.; Siva, A.; Nair, B. U. *Chem. Commun.* **2014**, *50*, 6902.
(46) Juris, A.; Balzani, V.; Barigelletti, F.; Campagna, S.; Belser, P.; von Zelewsky, A. *Coord. Chem. Rev.* **1988**, *84*, 85.
(47) Kalyanasundaram, K. *Coord. Chem. Rev.* **1982**, *46*, 159.
(48) Hirakawa, A. Y.; Tsuboi, M. *Science* **1975**, *188*, 359.
(49) Caricato, M.; Mennucci, B.; Tomasi, J.; Ingrosso, F.; Cammi, R.; Corni, S.; Scalmani, G. *J. Chem. Phys.* **2006**, *124*, 124520.
(50) Improta, R.; Scalmani, G.; Frisch, M. J.; Barone, V. *J. Chem. Phys.* **2007**, *127*, 074504.
(51) Improta, R.; Barone, V.; Scalmani, G.; Frisch, M. J. *J. Chem. Phys.* **2006**, *125*, 054103.
(52) Santoro, F.; Improta, R.; Lami, A.; Bloino, J.; Barone, V. *J. Chem. Phys.* **2007**, *126*, 084509.
(53) Santoro, F.; Lami, A.; Improta, R.; Barone, V. *J. Chem. Phys.* **2007**, *126*, 184102.
(54) Cammi, R.; Corni, S.; Mennucci, B.; Tomasi, J. *J. Chem. Phys.* **2005**, *122*, 104513.
(55) Cammi, R.; Mennucci, B. *J. Chem. Phys.* **1999**, *110*, 9877.
(56) Caricato, M. *Comput. Theor. Chem.* **2014**, *1040*−*1041*, 99.
(57) Guido, C. A.; Jacquemin, D.; Adamo, C.; Mennucci, B. *J. Chem. Theory Comput.* **2015**, *11*, 5782.
(58) Bernini, C.; Zani, L.; Calamante, M.; Reginato, G.; Mordini, A.; Taddei, M.; Basosi, R.; Sinicropi, A. *J. Chem. Theory Comput.* **2014**, *10*, 3925.
(59) Wang, R. L.; Tam, K. Y.; Marken, F.; Compton, R. G. *Electroanalysis* **1997**, *9*, 284.
(60) Amthor, S.; Noller, B.; Lambert, C. *Chem. Phys.* **2005**, *316*, 141.
(61) Turró, C.; Chung, Y. C.; Leventis, N.; Kuchenmeister, M. E.; Wagner, P. J.; Leroi, G. E. *Inorg. Chem.* **1996**, *35*, 5104.
(62) Wąsik, R.; Wińska, P.; Poznański, J.; Shugar, D. *J. Phys. Chem. B* **2012**, *116*, 7259.
(63) Gillard, R. D.; Hill, R. E. E.; Maskill, R. *J. Chem. Soc. A* **1970**, 1447.
(64) Gottlieb, H. E.; Kotlyar, V.; Nudelman, A. *J. Org. Chem.* **1997**, *62*, 7512.
(65) *CrysAlisPro*, Version 1.171.36.28; Agilent Technologies: Yarnton, Oxfordshire, UK, 2013.

DOI: 10.1021/acs.inorgchem.6b01039
Inorg. Chem. XXXX, XXX, XXX−XXX

(66) Sheldrick, G. M. *SHELX-97*; Programs for Crystal Structure Analysis: Göttingen, Germany, 1998.
(67) Sheldrick, G. M. *Acta Crystallogr., Sect. A: Found. Crystallogr.* **2008**, *64*, 112.
(68) Noviandri, I.; Brown, K. N.; Fleming, D. S.; Gulyas, P. T.; Lay, P. A.; Masters, A. F.; Phillips, L. *J. Phys. Chem. B* **1999**, *103*, 6713.
(69) Horvath, R.; Fraser, M. G.; Cameron, S. A.; Blackman, A. G.; Wagner, P.; Officer, D. L.; Gordon, K. C. *Inorg. Chem.* **2013**, *52*, 1304.
(70) Howell, S. L.; Gordon, K. C. *J. Phys. Chem. A* **2004**, *108*, 2536.
(71) Lind, S. J.; Gordon, K. C.; Waterland, M. R. *J. Raman Spectrosc.* **2008**, *39*, 1556.
(72) Lind, S. J.; Gordon, K. C.; Gambhir, S.; Officer, D. L. *Phys. Chem. Chem. Phys.* **2009**, *11*, 5598.
(73) Kim, K.; Jordan, K. D. *J. Phys. Chem.* **1994**, *98*, 10089.
(74) Becke, A. D. *J. Chem. Phys.* **1993**, *98*, 5648.
(75) Lee, C.; Yang, W.; Parr, R. G. *Phys. Rev. B: Condens. Matter Mater. Phys.* **1988**, *37*, 785.
(76) Hay, P. J.; Wadt, W. R. *J. Chem. Phys.* **1985**, *82*, 299.
(77) Hay, P. J.; Wadt, W. R. *J. Chem. Phys.* **1985**, *82*, 270.
(78) Wadt, W. R.; Hay, P. J. *J. Chem. Phys.* **1985**, *82*, 284.
(79) Petersson, A.; Bennett, A.; Tensfeldt, T. G.; Al-Laham, M. A.; Shirley, W. A.; Mantzaris, J. *J. Chem. Phys.* **1988**, *89*, 2193.
(80) Petersson, G.; Al-Laham, M. A. *J. Chem. Phys.* **1991**, *94*, 6081.
(81) Yanai, T.; Tew, D. P.; Handy, N. C. *Chem. Phys. Lett.* **2004**, *393*, 51.
(82) Barone, V.; Cossi, M.; Tomasi, J. *J. Chem. Phys.* **1997**, *107*, 3210.
(83) Cossi, M.; Barone, V.; Cammi, R.; Tomasi, J. *Chem. Phys. Lett.* **1996**, *255*, 327.
(84) Kirkwood, J. G. *J. Chem. Phys.* **1934**, *2*, 351.
(85) Tomasi, J.; Mennucci, B.; Cammi, R. *Chem. Rev.* **2005**, *105*, 2999.
(86) O'Boyle, N. M.; Tenderholt, A. L.; Langner, K. M. *J. Comput. Chem.* **2008**, *29*, 839.
(87) Horvath, R.; Gordon, K. C. *Coord. Chem. Rev.* **2010**, *254*, 2505.
(88) Schaftenaar, G.; Noordik, J. H. *J. Comput.-Aided Mol. Des.* **2000**, *14*, 123.

DOI: 10.1021/acs.inorgchem.6b01039
Inorg. Chem. XXXX, XXX, XXX−XXX